

TD-DFT Calculations, NBO, NLO Analysis and Electronic Absorption Spectra of Some Novel Thiazolo[3,2-a]Pyridine Derivatives Bearing Anthracenyl Moiety

Shimaa Abdel Halim Hussien

Department of Chemistry, Faculty of Education, Ain Shams University, Cairo, Egypt

Email address:

Shimaaquantum@ymail.com

To cite this article:

Shimaa Abdel Halim Hussien. TD-DFT Calculations, NBO, NLO Analysis and Electronic Absorption Spectra of Some Novel Thiazolo[3,2-a]Pyridine Derivatives Bearing Anthracenyl Moiety. *International Journal of Computational and Theoretical Chemistry*.

Vol. 7, No. 1, 2019, pp. 65-86. doi: 10.11648/j.ijctc.20190701.19

Received: January 28, 2019; Accepted: March 21, 2019; Published: May 17, 2019

Abstract: The electronic structure and spectra of the studied compounds 1–4 are investigated using TD-DFT/B3LYB/6-311G (d, p) level of theory. The results of calculations show that all the studied compounds 1–4 are non-planar, as indicated from the dihedral angles. The electronic absorption spectra of the studied compounds are recorded in the UV-VIS region, in both Acetone (as polar solvent) and Xylene (as non-polar solvent). The observed vertical electronic transitions assignments are facilitated via time-dependent density functional theory TD-DFT. Solvent dependence of the band maxima (λ_{\max}) and intensities of the observed spectra are explained in terms of blue and red shifts. Electronic configurations contributing to each excited state are identified and the relevant MOs are characterized. The natural bond orbital (NBO) analysis were discussed in terms of the extent of delocalization, intermolecular charge transfer and second order perturbation interactions between donor and acceptor MOs. The Coulomb-attenuating method (CAM-B3LYP) and Corrected Linear Response Polarizable Continuum Model (CLR) PCM studied for theoretically obtaining the electronic absorption spectra in gas phase, Acetone and Xylene, respectively, indicate a good agreement with the observed spectra. The calculated nonlinear optical parameters (NLO); polarizability (α), anisotropy of the polarizability ($\Delta\alpha$) and first order hyperpolarizability (β) of the studied compounds show promising optical properties. The HOMO-LUMO energy gap helped in analyzing the chemical reactivity, hardness, softness, chemical potential and electro negativity. 3D-plots of the molecular electrostatic potential (MEP) for the studied compounds are investigated and analyzed showing the distribution of electronic density of orbital's describing the electrophilic and nucleophilic sites of the selected molecules.

Keywords: UV Spectra, TD-DFT, Solvent and Substituent Effects, NBO and NLO Analysis

1. Introduction

The novel structure may be used in designing new potent and less toxic antimicrobial agents. Nitrogen-containing heterocyclic compounds have a diverse range of biological and pharmacological properties [1–4]. Thiazolo[3,2-a]pyridines, containing two fused heterocyclic rings, also; it's found in medicinal chemistry as they have an excellent biological activity with a wide range of applications, including antimicrobial [5], antiviral [6] antihypertensive [7], antihistaminic [8], neurotropic [9], anticonvulsant [10], antidepressant, sedative, analgesic [11,12] and anti-cancer activities. Among the various of anthraquinones are

identified also biologically active compounds. A lot of anthraquinone compounds are found in plants, microorganisms [13], among of them are natural antibiotics anthracyclines [14] and cidamicines [15]. Recently, anthracene derivatives actively began to gain new application areas such as biologically active agents, analytical reagents [16–18], phosphors [19], the components of liquid crystal compositions, photo materials, chemical additives for polymeric materials and they have found their application in color photography and electrophotography, laser technology, LCD and photochromic materials [20, 21].

The newly synthesized thiazolo[3,2-a]Pyridines having anthracenyl moiety derivatives 1-4 are expected to have

biological potential which needs to be explored by investigating their electronic structure and spectra experimentally and theoretically. The UV spectra, NLO and NBO analysis have been used to explain charge transfer within these molecules. The dependence on the electronic transitions to these molecules on the polarity of the solvent can be inferred from solvent-induced changes of such transitions, which is known as solvatochromism Corrected Linear Response Polarizable Continuum Model (CLR) PCM.

In continuation to our previous work [22-24], the objective of the present study aims to the calculations of density functional theory (DFT) and time-dependent density functional theory (TD-DFT) by using B3LYP at the 6-311G(d,p) basis set to obtain geometries, electronic structures, non liner optical properties (NLO), natural bonding orbital's (NBO), UV-Vis spectra, and molecular electrostatic potential contours of the studied compounds 1–4, these parameters characterize the forces that govern the structure of the studied compounds 1–4. The hybridization of each atom, natural charges, bonding and antibonding orbital's second order perturbation energy ($E(2)$), exact configurations and Lewis and non-Lewis electrons results from natural bonding orbital analysis. The present work attempts to provide a detailed experimental (UV) and theoretical electronic structure and spectra of the studied compounds 1–4 using CAM- B3LYP/6-311G (d, p). The origin of each absorption band is identified and the contributing configurations and MOs are characterized. The identify the extent of delocalization and the charge transfer of the electron density in the studied molecular systems by Natural bond orbital analysis (NBO) and also; extent of conjugative interaction between different subsystems of the studied compounds. The effect of solvent polarity on the observed spectra and hence, predicting the relative stabilities, extent of charge transfers character and assignment of the observed electronic transitions are analyzed. The effect substituent's of different electron donating groups ($X = \text{CH}_3$ and $X = \text{OCH}_3$) and electron withdrawing groups ($X = \text{Cl}$) on the electronic spectra of the studied compounds are discussed and analyzed. The molecular electrostatic potential (MEP) of the studied molecules were explored as well

2. Experimental

2.1. Compounds

The structure of the four proposed molecules 1–4 of Anthranlyl Thiazolo[3,2-a]Pyridine derivatives, is shown below, where compound 1 is 5-amino-2 (anthracen-9-ylmethylene)-3-oxo-7-phenyl-2,3-dihydro-7H-thiazolo[3,2-a]pyridine-6,8 dicarbonitrile, compound 2 is 5-amino-2-(anthracen-9-ylmethylene)-3-oxo-7-(p-tolyl) 2,3-dihydro-7H-thiazolo[3,2-a]pyridine-6,8-dicarbonitrile, compound 3 is 5-amino-2 (anthracen-9-ylmethylene)-7-(4-methoxyphenyl)-3-oxo-2,3-dihydro-7H-thiazolo[3,2-a]pyridine-6,8-dicarbonitrile, and compound 4 is 5-amino-2-(anthracen-9-ylmethylene) 7-(4-chlorophenyl)-3-oxo-2,3-dihydro-7H-

thiazolo[3,2-a]pyridine-6,8-dicarbonitrile.

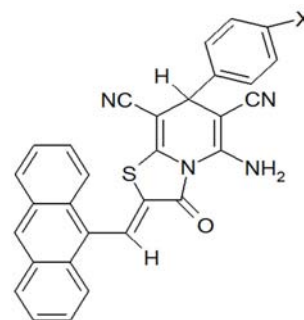


Figure 1. The structure of the four proposed molecules 1–4 of Anthranlyl Thiazolo[3,2-a]Pyridine derivatives.

Table 1. The structure of the four proposed molecules 1–4 of Anthranlyl Thiazolo[3,2-a]Pyridine derivatives.

Compounds	X
1	H
2	CH ₃
3	OCH ₃
4	Cl

2.2. Solvents

Polar (acetone) and non-polar (xylene) solvents were obtained from Merck, AR- grade, and were used without further purification.

2.3. Apparatus

A Perkin Elmer lambda 4B spectrophotometer using 1.0 cm fused quartz cells were used to measured the electronic absorption spectra over the range 200-900 nm.

2.4. Computational Details

All computations were carried out using Khon-Sham's DFT method subjected to the gradient-corrected hybrid density functional B3LYP method [25]. This function is a combination of the Becke's three parameters non-local exchange potential with the non-local correlation functional of Lee et al [26]. For each structure, a full geometry optimization was performed using this function [26] and the 6-311G (d, p) bases set [27] as implemented by Gaussian 09 package [28]. All geometries were visualized either using GaussView 5.0.9 [29] or chemcraft 1.6 [30] software packages. No symmetry constrains were applied during the geometry optimization. Also, the total static dipole moment (μ), $\langle \alpha \rangle$, and $\langle \beta \rangle$, values were calculated by using the following equations [31-33]:

$$\mu = (\mu_x^2 + \mu_y^2 + \mu_z^2)^{1/2},$$

$$\langle \alpha \rangle = 1/3 (\alpha_{xx} + \alpha_{yy} + \alpha_{zz}),$$

$$\Delta \alpha = ((\alpha_{xx} - \alpha_{yy})^2 + (\alpha_{yy} - \alpha_{zz})^2 + (\alpha_{zz} - \alpha_{xx})^2/2)^{1/2},$$

$$\langle \beta \rangle = (\beta_x^2 + \beta_y^2 + \beta_z^2)^{1/2}, \quad (1)$$

Where

$$\begin{aligned}\beta_x &= \beta_{xxx} + \beta_{xyy} + \beta_{xzz}, \\ \beta_y &= \beta_{yyy} + \beta_{xxy} + \beta_{yyz}, \\ \beta_z &= \beta_{zzz} + \beta_{xxz} + \beta_{yyz}.\end{aligned}\quad (2)$$

The electronic transition properties which include the maximum excitation wavelength (λ_{\max}) and relative intensities (oscillator strengths, f), were obtained by the time dependant density functional theory (TD-DFT), [34] using "A new hybrid exchange-correlation functional using the Coulomb-attenuating method (CAM-B3LYP)," at the 6-311G (d, p) bases set [35]. The population analysis has also been performed by the natural bond orbital method [36] at B3LYP/6-311G (d, p) level of theory using natural bond orbital (NBO) under Gaussian 09 program package. The second-order Fock matrix was used to evaluate the donor-acceptor interactions in the NBO basis [37]. For each donor (i) and acceptor (j), the stabilization energy $E^{(2)}$ associated with the delocalization $i \rightarrow j$ is estimated as

$$E^{(2)} = \Delta E_{ij} = q_i (F_{ij})^2 / (\epsilon_j - \epsilon_i), \quad (3)$$

Where q_i is the donor orbital occupancy, ϵ_i and ϵ_j are diagonal elements and (ij) is the off-diagonal NBO Fock matrix element. For the conversion factors of α , β , and HOMO and LUMO energies in atomic and cgs units: 1 atomic unit (a.u.) = 0.1482×10^{-24} electrostatic unit (esu) for polarizability $\langle\alpha\rangle$; 1 a.u. = 8.6393×10^{-33} esu for first hyperpolarizability $\langle\beta\rangle$; 1 a.u. = 27.2116 eV for HOMO and LUMO energies.

3. Result and Discussion

3.1. Electronic Structure

3.1.1. Geometry Structure

Figures 2-4, presents the optimized structures of the

studied compounds 1-4, numbering system, HOMO and LUMO-charge density maps and the vector of dipole moment using the B3LYB/6-311G (d, p). From "Figures 2-4, it is obvious that, the optimized structures of the studied compounds, 1-4, is non-planer with the phenyl ring at C₃ and anthranyl moiety at C₉ are out of the molecular plane of novel thiazolo[3,2-a]Pyridines having anthranyl moiety by a dihedral angles of 111° and 128° respectively. The insertion of X= p-Cl, p-CH₃, and p-OCH₃ at C₃-ph does not change the geometry of the studied compounds 1-4 "Figure 2". This may be attributed to that the phenyl at C₃ and anthranyl moiety at C₉ are out of the molecular plane.

The optimized geometric parameters (bond lengths, bond angles and dihedral angles) of the parent molecule 1 and some of its derivatives 2-4 using B3LYP/6-311G (d,p) method are listed in Tables 2 and 3. The optimized bond lengths and bond angles are compared with the available X-ray experimental data [38-40]. The observed bond lengths of C₁-C₂ and C₂-C₃ in pyridine ring are 1.371Å and 1.521Å respectively, while the theoretical values are 1.370Å and 1.518Å respectively. For C-S bonds (C₅-S₈ and S₈-C₉), the calculated values are greater than the experimental values by 0.045Å and 0.014Å respectively. There is a great agreement between the calculated bond lengths of the parent 1 and the experimental values indicating the power of the method used. For derivative 2, the calculated bond angles <C4C5S8 (124.85°) and <N6C10C9 (110.24°) are overestimated than the experimental values, whereas, the calculated bond angles <C5N6C1 (119.23°) and <N6C5S8 (111.86°) are underestimated than the experimental values (c.f. Table 2). The effect of different substituent's in the derivatives 3 and 4 are listed in Table 2. There are disagreement between the calculated bond angle and the experimental values which may be attributed to that the calculation were carried out in the gas phase and the experimental measured in the solid state. All the studied compounds 2a-d are non-planner as indicating from the calculated dihedral angles (c.f. Table 3).

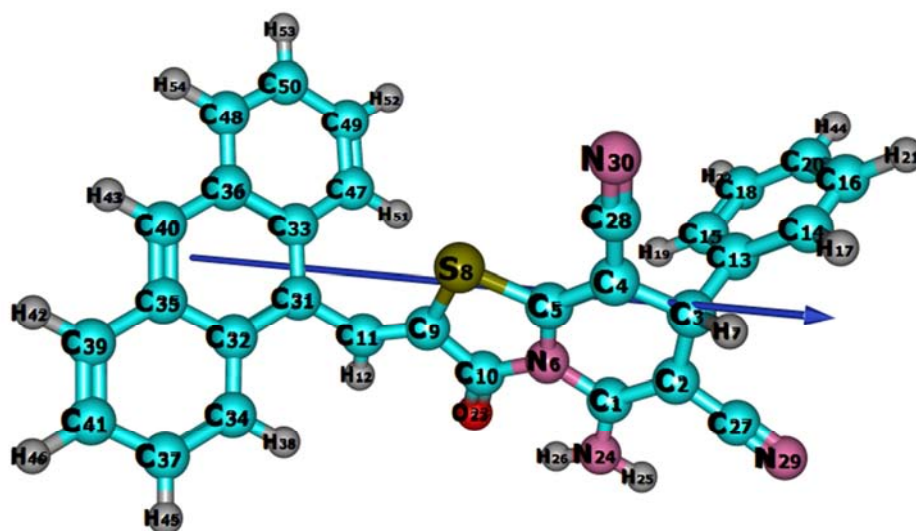
Table 2. Selected experimental and theoretical bond lengths, and bond angles for the studied compounds (1-4) computed at the B3LYP/6-311G(d,p) level of theory.

Parameters	EXP.[38-40]	1	2	3	4
Bond lengths (Å)					
C ₁ -C ₂	1.371	1.370	1.370	1.370	1.370
C ₂ -C ₃	1.521	1.518	1.518	1.518	1.517
C ₄ -C ₅	1.341	1.349	1.349	1.349	1.349
C ₅ -N ₆	1.389	1.402	1.402	1.402	1.402
C ₁ -N ₆	1.387	1.420	1.420	1.420	1.420
C ₅ -S ₈	1.722	1.767	1.767	1.768	1.766
S ₈ -C ₉	1.753	1.767	1.767	1.767	1.768
C ₉ -C ₁₀	1.399	1.481	1.481	1.482	1.480
C ₉ -C ₁₁	1.341	1.346	1.346	1.346	1.347
C ₁₁ -C ₃₁	1.451	1.468	1.468	1.468	1.467
C ₁₀ -N ₆	1.412	1.406	1.406	1.405	1.407
C ₁₀ -O ₂₃	1.290	1.217	1.217	1.217	1.217
C ₁ -N ₂₄	1.345	1.354	1.355	1.356	1.354
C ₂ -C ₂₇	1.389	1.414	1.414	1.414	1.414
C ₂₇ -N ₂₉	1.190	1.159	1.159	1.159	1.159
C ₃ -C ₁₃	1.524	1.533	1.532	1.531	1.533

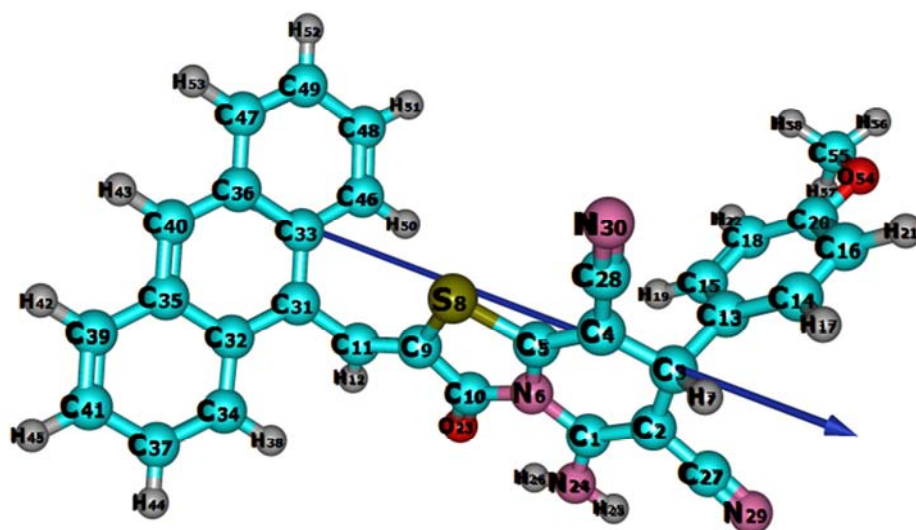
Parameters	EXP.[38-40]	1	2	3	4
C ₄ – C ₂₈	1.412	1.419	1.419	1.419	1.419
C ₂₈ – N ₃₀	1.190	1.157	1.157	1.157	1.157
Bond Angles (°)					
<N ₆ -C ₁ -C ₂	120.00	119.31	119.29	119.31	119.31
<C ₁ -C ₂ -C ₃	124.99	124.89	124.87	124.91	124.81
<C ₂ -C ₃ -C ₄	109.31	109.82	109.75	109.71	109.82
<C ₃ -C ₄ -C ₅	121.00	122.28	122.26	122.28	122.20
<C ₄ -C ₅ -S ₈	123.99	124.85	124.90	124.93	124.86
<C ₄ -C ₅ -N ₆	123.95	123.29	123.26	123.26	123.26
<C ₅ -N ₆ -C ₁	119.80	119.23	119.22	119.20	119.25
<N ₆ -C ₅ -S ₈	110.96	111.86	111.84	111.81	111.88
<N ₆ -C ₁₀ -C ₉	109.55	110.24	110.26	110.27	110.25
<S ₈ -C ₉ -C ₁₀	110.69	111.39	111.37	111.36	111.38
<C ₉ -S ₈ -C ₅	95.411	91.102	91.102	91.110	91.107
<C ₁₁ -C ₉ -S ₈	130.81	127.94	127.98	128.10	128.03
<C ₉ -C ₁₁ -C ₃₁	127.99	128.40	128.45	128.67	128.67
<C ₉ -C ₁₀ -O ₂₃	124.61	124.82	124.81	124.79	124.92
<O ₂₃ -C ₁₀ -N ₆	125.00	124.94	124.93	124.94	124.83
<C ₁₀ -N ₆ -C ₁	125.00	125.36	125.36	125.36	125.34
<N ₆ -C ₁ -N ₂₄	115.92	116.23	116.23	116.22	116.31
<N ₂₄ -C ₁ -C ₂	125.00	124.39	124.40	124.40	124.32
<C ₁ -C ₂ -C ₂₇	116.95	117.11	117.11	117.06	117.18
<C ₂ -C ₂₇ -N ₂₉	177.99	178.15	178.16	178.10	178.28
<C ₂ -C ₃ -C ₁₃	113.69	112.10	112.10	113.18	113.06
<C ₄ -C ₃ -C ₁₃	113.36	111.25	111.28	111.30	111.06
<C ₃ -C ₄ -C ₂₈	117.96	118.27	118.26	118.27	118.22
<C ₄ -C ₂₈ -N ₃₀	177.99	179.17	179.15	179.14	179.05

Table 3. Dihedral Angles (°) and Natural Charge for the studied compounds (1-4) computed at the B3LYP/6-311G(d,P) level of theory.

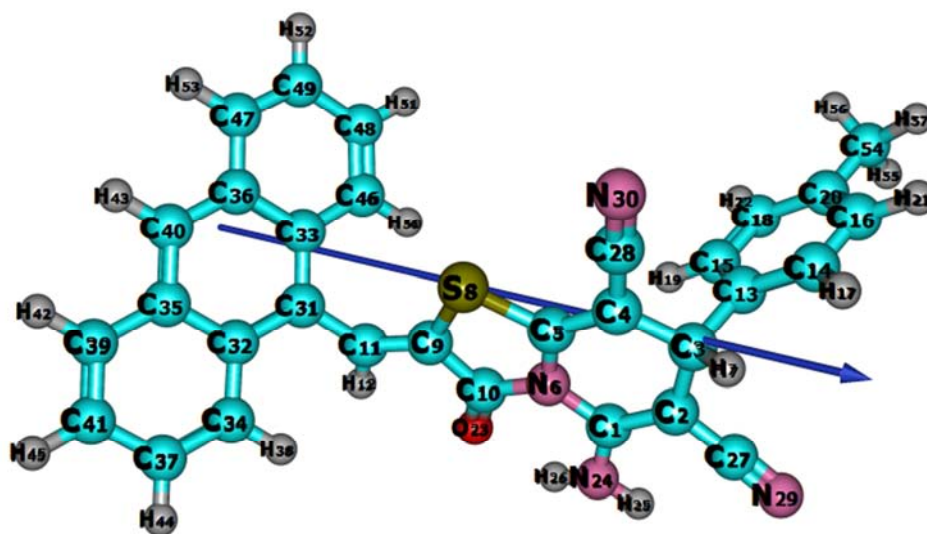
Parameters	1	2	3	4
Dihedral Angles (°)				
<C ₁ C ₂ C ₃ C ₄	9.324	10.094	10.031	10.150
<C ₃ C ₄ C ₅ N ₆	3.255	3.534	3.712	3.641
<C ₄ C ₅ N ₆ C ₁	6.323	6.669	6.572	6.640
<C ₄ C ₅ S ₈ C ₉	177.72	177.44	177.24	177.55
<N ₆ C ₅ S ₈ C ₉	-1.474	-1.670	-1.834	-1.612
<S ₈ C ₉ C ₁₁ C ₃₁	1.044	0.969	0.972	1.130
<S ₈ C ₉ C ₁₀ N ₆	1.538	1.511	1.150	1.058
<O ₂₃ C ₁₀ N ₆ C ₁	-5.148	-5.266	-5.059	-5.225
<C ₁₀ N ₆ C ₁ N ₂₄	-7.091	-7.518	-7.634	-6.924
<N ₆ C ₁ N ₂₄ H ₂₅	173.43	173.10	173.11	173.73
<C ₁ C ₂ C ₂₇ N ₂₉	-9.194	-9.633	-7.939	-8.454
<C ₃ C ₄ C ₂₈ N ₃₀	-54.427	-55.646	-57.167	-42.223
<C ₁₃ C ₃ C ₄ C ₂₈	-63.119	-63.658	-63.350	-63.796
<C ₁₃ C ₃ C ₂ H ₇	118.034	118.088	118.095	118.128
<C ₉ C ₁₁ C ₃₁ H ₁₂	-175.43	-175.40	-175.40	-175.41
Natural Charge				
C1	0.4622	0.4615	0.4598	0.4633
C2	-0.2796	-0.2794	-0.2778	-0.2838
N6	-0.4702	-0.4701	-0.4691	-0.4705
S8	0.4004	0.3998	0.3987	0.4024
C9	-0.2673	-0.2668	-0.2675	-0.2689
C10	0.6842	0.6851	0.6839	0.6851
O23	-0.6064	-0.6077	-0.6077	-0.6063
N24	-0.7677	-0.7678	-0.7696	-0.7661
N29	-0.3461	-0.3436	-0.3446	-0.3420
N30	-0.3037	-0.2990	-0.3008	-0.2960
C55	-----	-0.5835	-0.1977	-----
O54	-----	-----	-0.5216	-----
Cl54	-----	-----	-----	-0.0070



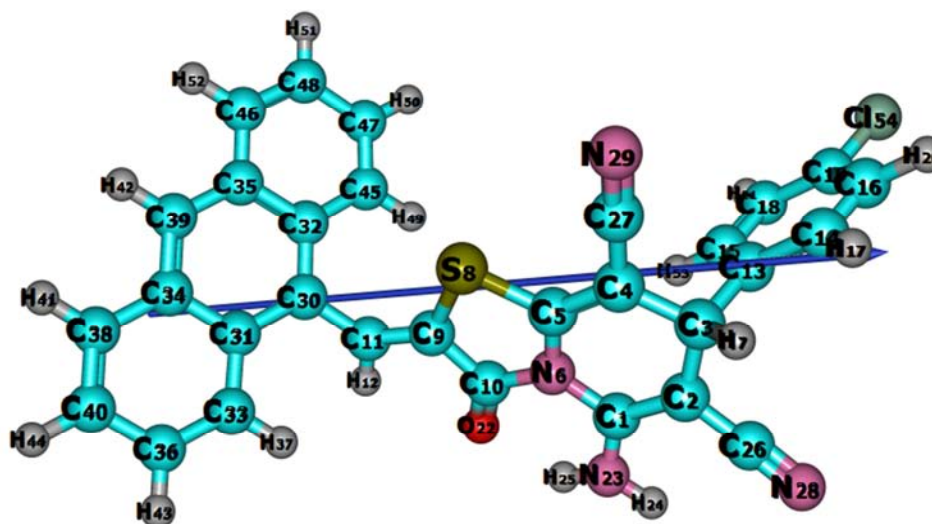
(1)



(2)



(3)



(4)

Figure 2. Optimized geometry, vector of the dipole moment and numbering system, for the studied compounds 1-4 at B3LYP/6-311G (d, p).

1			LUMO plot (first excited state) $E_{\text{LUMO}} = -2.8911\text{eV}$ $E_{\text{gap}} = 3.0116\text{eV}$ $E_{\text{HOMO}} = -5.9027\text{eV}$ HOMO plot (ground state) HOMO and LUMO energy band gap
	HOMO	LUMO	
2			LUMO plot (first excited state) $E_{\text{LUMO}} = -2.8693\text{eV}$ $E_{\text{gap}} = 3.0167\text{eV}$ $E_{\text{HOMO}} = -5.8861\text{eV}$ HOMO plot (ground state) HOMO and LUMO energy band gap
	HOMO	LUMO	
3			LUMO plot (first excited state) $E_{\text{LUMO}} = -2.8669\text{eV}$ $E_{\text{gap}} = 3.0140\text{eV}$ $E_{\text{HOMO}} = -5.8809\text{eV}$ HOMO plot (ground state) HOMO and LUMO energy band gap
	HOMO	LUMO	
4			LUMO plot (first excited state) $E_{\text{LUMO}} = -2.9781\text{eV}$ $E_{\text{gap}} = 2.9841\text{eV}$ $E_{\text{HOMO}} = -5.9622\text{eV}$ HOMO plot (ground state) HOMO and LUMO energy band gap
	HOMO	LUMO	

Figure 3. HOMO, LUMO maps and energy gap of 1-4 at B3LYP/6-311G (d, p).

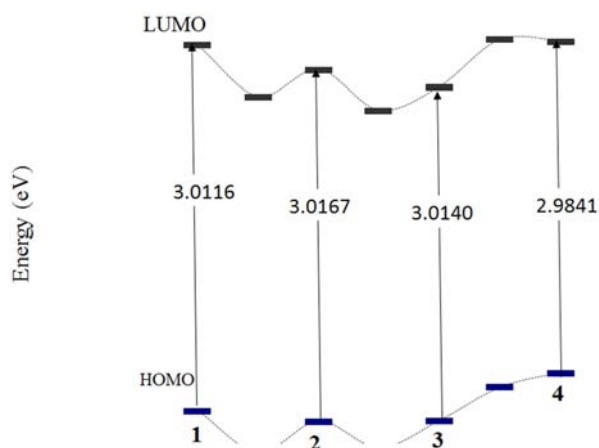


Figure 4. Energy of HOMO, LUMO and energy gap of the studied compounds 1-4 at B3LYP/6-311G(d,p) level of theory.

3.1.2. Ground State Properties

The ionization energy, I , of compound 1 which measures the donating property (oxidation power) is 5.90 eV (c.f. Table 4). The effect of substituent's of different strengths and hence in the donating properties follows the order: $3 > 2 > 1 > 4$, as shown in Table 4 and "Figures 3 and 4". However the electron affinity, A , of 1 which measures the accepting property (reducing power) is 2.89 eV. The order of accepting properties of novel thiazolo[3,2-a]Pyridines having

anthranyl moiety derivatives follows $3 < 2 < 1 < 4$, as shown in Table 4 and "Figure 4". The band gap, E_{gap} , is the energy gap between E_{HOMO} and E_{LUMO} , it signifies the facile electron transition from E_{HOMO} to E_{LUMO} , i.e. the reactivity of molecules in the studied compounds 1-4 are governed by their chemical structures. The results in Table 4 and "Figure 4", shows that the computed reactivity in the gas phase of the studied compounds increases in the order: $4 > 1 > 3 > 2$. This indicates that the smaller the E_{gap} , the higher the reactivity of these compounds. The derivatives 2 and 3, the calculated E_{gap} are greater (less reactive) than the parent 1 by about ≈ 0.2 and 0.06 kcal/mol respectively, while the derivative 4, the computed E_{gap} are lower (high reactive) than the parent 2a by 0.027 eV (≈ 0.63 kcal/mol). Therefore, all functions must be attached to the fused thiazolo[3,2-a]pyridine the parent molecule leading to its reactivity. Finally, the theoretically computed dipole moment, μ , for compound 1 which measures the charge separation over the molecule is 6.62 D. The general trend of the dipole moment changes for the studied compounds 1-4 follow the order $4 > 3 > 1 > 2$ (c.f. Table 4) and the vector of the dipole moment is presented in "Figure 2". From the computed dipole moment, it's found that the presence of two cyano groups at C_2 and C_4 and anthracene group at C_9 (c.f. "Figures 2 and 3") are responsible for the polarity of the compound 1 (c.f. Table 2).

Table 4. Total energy, energy of HOMO and LUMO, energy gap, dipole moment, The ionization potential (I / eV), electron affinity (A / eV), chemical hardness (η / eV), global softness (S / eV⁻¹), chemical potential (V / eV⁻¹), electronegativity (χ / eV), and global electrophilicity index, (ω / eV), of the studied compounds (1-4) computed at the B3LYP/6-311G(d,p).

Compounds	1	2	3	4
E_T (au)	-1846.7984	-1886.1263	-1961.3519	-2306.4198
E_{HOMO} (eV)	-5.90267	-5.88608	-5.88091	-5.96224
E_{LUMO} (eV)	-2.89109	-2.86933	-2.86688	-2.97813
E_{gap} (eV)	3.01158	3.01675	3.01403	2.98411
μ (Debye)	6.6222	6.3840	7.2805	8.0169
I (eV)	5.90267	5.88608	5.88091	5.96224
A (eV)	2.89109	2.86933	2.86688	2.97813
χ (eV)	4.39688	4.37770	4.37389	4.47018
V (eV ⁻¹)	-4.39688	-4.37770	-4.37389	-4.47018
η (eV)	1.50579	1.50837	1.50701	1.49206
S (eV ⁻¹)	0.33205	0.33148	0.33178	0.33511
ω (eV)	6.41940	6.35261	6.34729	6.69630

3.1.3. Natural Charge

The natural population analysis [41] performed on the electronic structures of compounds 1-4 clearly describes the distribution of electrons in various sub-shells of their atomic orbits. The accumulations of charges on the individual atom presented in Table 3. In case of our studied compounds 1-4, the most negative centers are N6, O23, N24, N29, N30, O54, and C154-atoms. According to an electrostatic point of view of the molecule, these negative atoms have a tendency to donate an electron. Whereas, the most electropositive atoms such as; S8 have a tendency to accept an electron. These distributions of partial charges on the skeletal atoms show that the electrostatic repulsion or attraction between atoms

can give a significant contribution to the intra- and intermolecular interaction.

3.2. Global Reactivity Descriptors

They include HOMO, LUMO, energy gap (E_g), chemical hardness (η), electronegativity (χ), chemical potential (V), electrophilicity (ω), electron affinity (A), ionization potential (I) and global softness (S) which are calculated at B3LYP/6-311G(d,p). The frontier molecular orbital (FMO) energies of the studied compounds were calculated at the same level of theory. HOMO energy characterizes the electron donating ability, while LUMO energy characterizes the electron withdrawing ability. Energy gap (E_g) between

HOMO and LUMO characterizes the molecular chemical stability which is a critical parameter in determining molecular electrical transport properties because it is a measure of electron conductivity. The results in "Figure 3". and Table 4 indicate that the smaller the energy gap the easier the charge transfer and the polarization occurs within the molecule. Furthermore, the order of increasing reactivity in the studied compounds is: $4 > 1 > 3 > 2$. The insignificant differences in E_g of all the studied compounds except 4 is due to the non-planarity of the two ph-X and anthracene group with the thiazolo[3,2-a]pyridine moiety (c.f. Table 4). Using HOMO and LUMO energies, ionization potential and electron affinity can be expressed as $I \sim E_{\text{HOMO}}$, $A \sim E_{\text{LUMO}}$ at the B3LYP/6-311G (d,p) as shown in (Table 4). The variation of electronegativity (X) values is supported by electrostatic potential, for any two molecules, where electron will be partially transferred from one of low X to that of high X . The results show that the order of decreasing X is: $4 < 1 < 2 < 3$. The chemical hardness (η) = $(I-A)/2$, electronegativity (X) = $(I+A)/2$, chemical potential (V) = $-(I+A)/2$, electrophilicity (ω) = $\mu^2/2\eta$ and global softness (S) = $1/2\eta$ values are calculated and presented in Table 4. The results of small η values for the studied compounds reflect the ability of charge transfer inside the molecule. Therefore, the order is: $4 > 1 > 3 > 2$. There is a linear relationship between η and E_g as shown in (Table 4). Considering η values, the higher the η values, the harder is the molecule and vice versa.

3.3. Nonlinear Optical (NLO) Analysis

Non-linear optical properties are the ability of any compound to convert light of longer wave length into light of shorter wave length. Most applications of single crystals of any non linear materials are evident in the fields of semiconductors, infrared detectors, solid state lasers, photosensitive materials and crystalline thin films for microelectronics [42]. The investigation of the relationship between the electronic structure and NLO, parameters of the studied compounds 1-4 are calculated theoretically by using DFT/B3LYP/6-311G (d,p). Total static dipole moment (μ), the mean polarizability α , the anisotropy of the polarizability $\Delta\alpha$, the mean first-order hyperpolarizability (β) of the studied compounds 1-4 are listed in Table 5. In this study, P-nitro aniline (PNA) is a standard prototype molecule used in NLO studies, its chosen as a reference as there were no experimental values of NLO properties of the studied compounds. The values of α , β in Table 5 show that the order of increasing α with respect to PNA is: compounds 3 and 2 are ~ 3.5 and 3 times higher than (PNA), whereas compounds 4 and 1 are ~ 3 times higher than the standard (PNA) respectively, The calculated first order hyperpolarizability of p- nitroacetanilide (PNA) is 15.5×10^{-30} esu as reported by T. Gnanasambandan et al [43-45]. The analysis of the β parameter show that compounds 1 and 3 are ~ 2 times higher than (PNA), while compounds 2, and 4 are ~ 1.5 times higher than the reference respectively. Therefore, the studies compounds show promising optical properties.

Table 5. Total static dipol moment (μ), the mean polarizability ($\langle\alpha\rangle$), the anisotropy of the polarizability ($\Delta\alpha$), and the mean first-order hyperpolarizability ($\langle\beta\rangle$), for the studied compounds (1-4) computed at B3LYP/6-311G(d,P).

Property	PNA	1	2	3	4
μ_x , D		-2.3970	-2.19358	-2.25501	-1.96204
μ_y , D		0.22663	0.53737	0.86366	0.32376
μ_z , D		-0.98272	-1.08832	-1.53756	-0.62330
μ , Debye ^a	2.44	2.60052	2.506992	2.862706	2.083967
α_{xx} , a.u.		610.816	637.430	647.415	631.077
α_{xy} , a.u.		38.9403	37.7679	32.4371	37.9918
α_{yy} , a.u.		424.426	436.336	439.636	426.157
α_{zz} , a.u.		-6.62195	-3.22879	3.51065	7.59677
α_{yz} , a.u.		-6.21531	-0.33418	7.56950	-1.12186
α_{xz} , a.u.		246.694	256.239	261.914	253.320
$\langle\alpha\rangle \times 10^{-24}$ esu ^b	22	63.33	65.70	66.64	64.74
$\Delta\alpha \times 10^{-24}$ esu		47.85	49.91	50.27	49.55
β_{xxx} , a.u.		-311.565	-254.708	-278.249	-205.497
β_{xxy} , a.u.		163.254	170.091	168.919	179.192
β_{xyy} , a.u.		-113.614	-126.586	-111.257	-106.845
β_{yyy} , a.u.		8.21341	42.3811	95.0644	21.8794
β_{xxz} , a.u.		70.4887	61.9425	2.81160	78.8312
β_{xyz} , a.u.		-7.3633	-15.2491	-54.4635	-6.1162
β_{yyz} , a.u.		-49.3368	-45.3843	-53.0683	-53.0622
β_{xzz} , a.u.		29.0944	33.8242	71.6342	32.3890
β_{yzz} , a.u.		-28.8070	-32.3737	-22.8372	-33.5310
β_{zzz} , a.u.		-41.7722	-46.8760	-61.9453	-46.7887
$\langle\beta\rangle \times 10^{-30}$ esu ^c	15.5	27.167	22.672	25.961	18.306

a, b, c PNA results are taken from references [43-45].

3.4. Molecular Electrostatic Potential (MEP)

The electrophilic and nucleophilic attack as well as hydrogen bonding interactions in any molecular system can be explained in terms of the charge transfer and natural charges on active sites of the studied molecules [46]. DFT/B3LYP/6-311G (d,p) method of calculation of studied molecules (1-4) are calculated 3D MEP and ESP from optimized molecular structure are shown in "Figures 5 and 6". Potential increases in the following order: red < orange <

yellow < green < blue [47,48]. The results show that, in case of **1** (X=Y=H) the negative region (red) is mainly over the N and O atomic sites, which is caused by the contribution of lone-pair electrons of nitrogen and oxygen atoms while the positive (blue) potential sites are around the hydrogen, sulfur and carbon atoms. A portion of the molecule that has negative electrostatic potential will be susceptible to electrophilic attack—the more negative the higher the tendency for electrophilic attack.

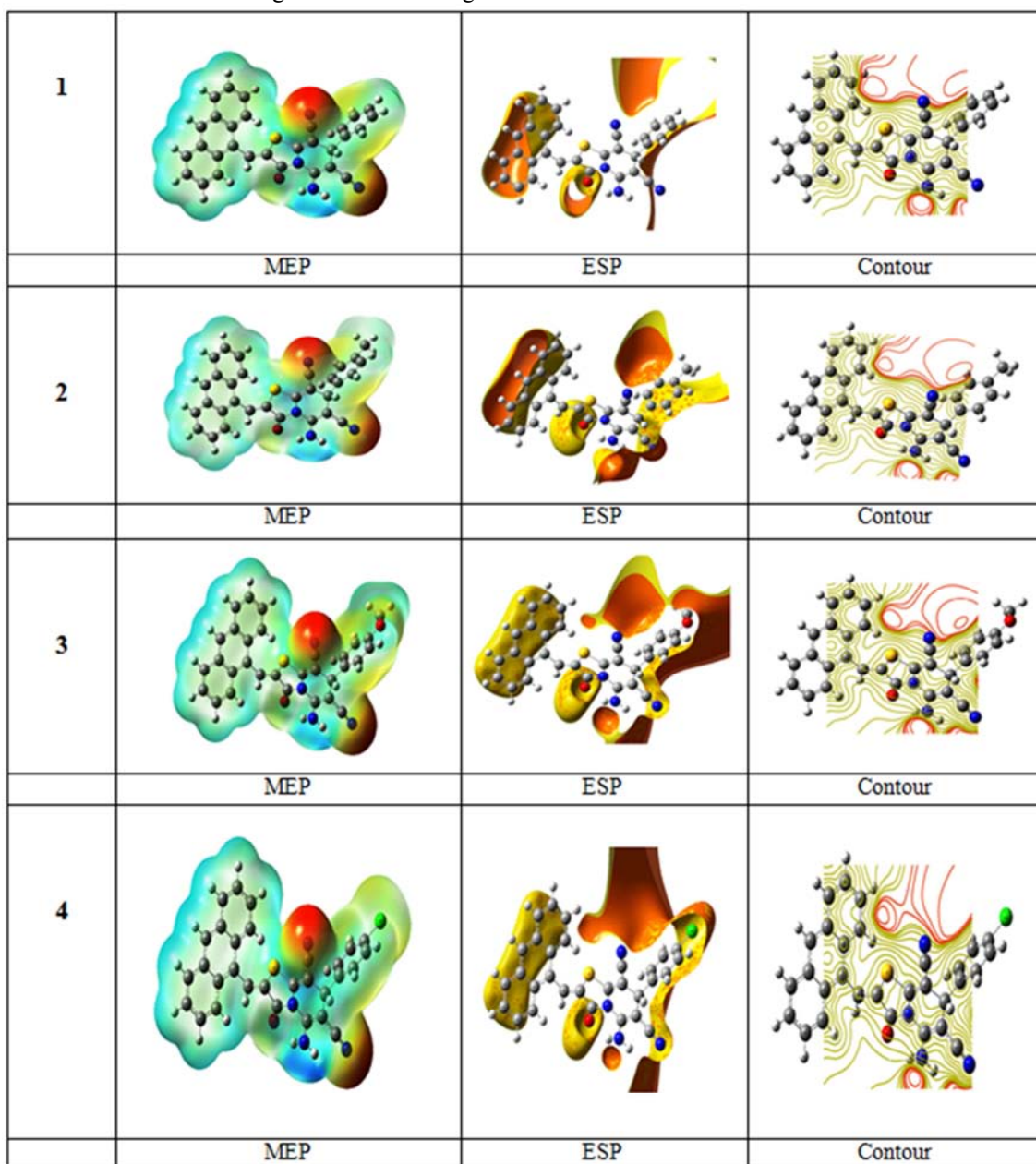


Figure 5. Molecular surfaces of studied compounds 1-4 at B3LYP/6-311G (d, p).

The color scheme for the MEP surface is as follows: red for electron rich, (partially negative charge); blue for electron deficient, (partially positive charge); light blue for (slightly electron deficient region); yellow for (slightly electron rich region); green for neutral (zero potential) respectively.

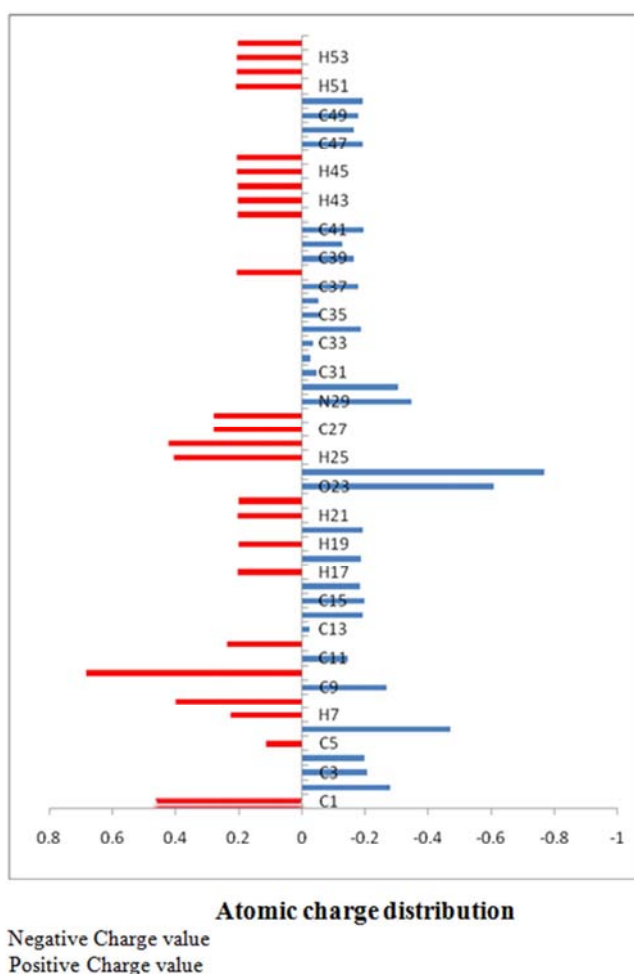


Figure 6. Atomic charge distribution (au) for 5-amino-2-(anthracen-9-ylmethylene)-3-oxo-7-phenyl-2,3-dihydro-7H-thiazolo[3,2-a]pyridine-6,8-dicarbonitrile 1 at B3LYP/6-311G(d,p) basis set.

3.5. Electronic Absorption Spectra of Anthranyl Thiazolo[3,2-a]Pyridine Derivatives

The electronic absorption spectra of novel thiazolo[3,2-a]Pyridines having anthranyl moiety derivatives studied in this work 1-4 depend on the type and extent of interaction between different moieties. The possible types of interaction between subsystems are presented in Figure 7. For example, (i) Cross

conjugation if no interaction between the fused thiazolo[3,2-a]pyridine and the terminal phenyl group Ph-X and the anthracene moiety, (ii) partial conjugation between Ph-X and Anthranyl Thiazolo[3,2-a]Pyridine, (iii) partial conjugation between anthracene moiety and Anthranyl Thiazolo[3,2-a]Pyridine (iv) full conjugation between the three subsystems Ph-X, anthracene moiety, and thiazolo[3,2-a]pyridine.

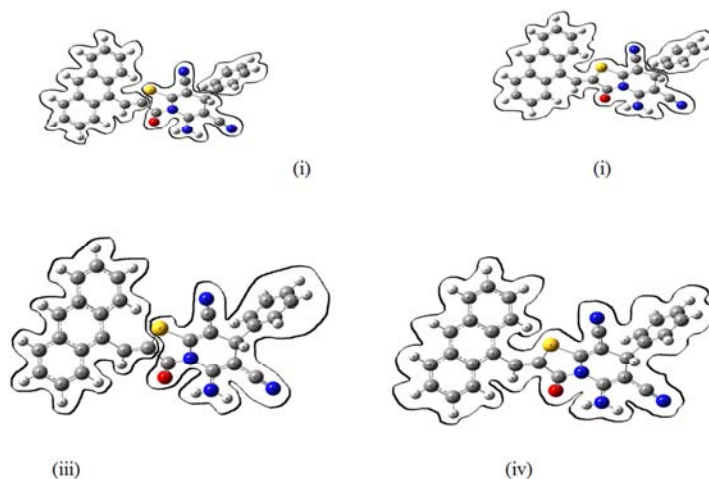


Figure 7. The types of conjugation between different moieties of Anthranyl Thiazolo[3,2-a]Pyridine.

3.5.1. Electronic Absorption Spectra of Compound 1

"Figure 8", and Table 7 presents the experimental and theoretical electronic absorption spectra of 1 in xylene and acetone. The spectrum of 1 is composed of three bands in the range 270–550 nm. The spectrum in xylene shows two intense bands at 418 nm, and 318 nm. Increasing solvent polarity on going from xylene to acetone results in a blue shift with the first band is shifted to 415 nm, and the second band is shifted to 313 nm, respectively. The two observed bands are assigned as (π – π^*) transitions, as indicated by the values of molar absorptivity (ϵ = 55000). Predicting and assigning the origin of the experimental spectrum of compound 1, one can calculate the theoretical gas phase transitions of the various subsystems a, b, and c as presented in "Figures 9-12", using CAM-B3LYP/6-311G (d, p). Five transitions are computed at 188.6, 234.6, 257.3, 312.4, and 371.8 nm for subsystem a; six transitions are computed at 129.4, 142.6, 168.5, 180.3, 218.0, and 235.9 nm for subsystem b; seven transitions are computed at 168.0, 187.7, 194.9, 232.2, 239.3, 260.6, and 283.6 nm for subsystem c; and five transitions are computed at 225.2, 251.5, 283.5, 310.7, and 403.8 nm for compound 1. The correlation of the theoretical transitions between the various subsystems show that the transition at 232.2, 260.6 and 283.6 nm of subsystem c correlates with the transition at 225.2, 251.5 and 283.5 nm of compound 1. Moreover, three transition at 234.6, 257.3, and 312.4 nm of subsystem a correlates with that at 225.2, 251.5 and 310.7 nm of compound 1. While, two transition at 218.0 and 235.9 nm of subsystem b correlates with that at 225.2 and 251.5 nm of compound 1. This indicates that the interaction of anthracene moiety and thiazolo[3,2-a]pyridine of subsystem c reproduces the partial conjugation (ii), which verifies the negligible influence of the interaction of Ph-X (c. f. Figure 7). In order to account for the experimentally observed UV Spectra of 1 in xylene and acetone, it is essential to consider the theoretically calculated vertical transitions using TD-DFT-CAM-B3LYP/6-311G (d, p) level. The experimental band at 418 nm (in xylene) is reproduced theoretically by using PCM (xylene), at 414 (state I) nm, and in gas phase at 403.8 nm as shown in Table 7. The theoretical calculations of single point energy vertical excitations in acetone reproduce the wavelength of this band at 412 nm (state I), indicating that the calculated wavelength is lower than the observed wavelength. The second band observed experimentally at 318

nm in xylene, is reproduced theoretically at 311 nm (state II). The gas phase calculation gives a wavelength at 310.7 nm. Moreover, In acetone, this same band appears at 313 nm, where theoretical calculations in acetone reproduce this band at 308 nm (state II), as shown in Table 7. The third (π – π^*)¹ state theoretically in xylene at 256 nm (state III), which involves the orbital's ϕ_{123} and ϕ_{127} , in the transition. The gas phase calculation gives a wavelength at 251.5 nm (state III), which also involves orbital's ϕ_{123} and ϕ_{127} . In acetone, this same band appears theoretically at 257 nm, (state III), as shown in Table 7. The nature of the electronic transition can be inferred from examining the electron density contours of molecular orbitals. The four orbital's ϕ_{123} , ϕ_{125} , ϕ_{126} , and ϕ_{127} respectively, involved in the theoretical transitions of 1, are shown in "Figure 13", where the first, second and third bands involving ϕ_{125} and ϕ_{126} & ϕ_{123} and ϕ_{127} show a delocalization of electron density, and Charge Transfer CT character.

The NBO analysis of the studied compounds 1-4 provides an efficient method for studying intra- and intermolecular bonding and also provides a convenient basis for investigating charge transfer or conjugative interactions in molecular systems. Table 6 presents the second order perturbation energies of most interacting NBOs of 1-4 and the most important interaction between filled (donor) Lewis type NBOs and empty (acceptor) non-Lewis NBOs. The charge density maps of HOMO and LUMO for 1-4 are presented in "Figure 13". The results of NBO analysis of compound 1 tabulated in Table 6 indicate that there is a strong hyper conjugative interactions $\pi^*C_9-C_{11} \rightarrow \pi^*C_{31}-C_{33}$, LP (1) $N_{24} \rightarrow \pi^*C_1-C_2$, LP (1) $N_6 \rightarrow \pi^*C_4-C_5$, LP (2) $O_{23} \rightarrow \sigma^*N_6-C_{10}$, and $\pi C_1-C_2 \rightarrow \pi^*C_{27}-N_{29}$, for 1 is 55.78, 51.82, 33.88, 26.81, and 23.58 kcal/mol, respectively. The C–N orbital in two cyano groups and amino group interacts equally well with pyridine ring. In fact, its interaction with the thiazolo ring is greater. Furthermore, the lone pair orbital of the nitrogen atom enjoys hyperconjugation with the $C_{10}-O_{23}$, and C_1-C_2 π^* orbital. The oxygen and sulfur lone pair orbital's, on the other hand, interact essentially with the C_5-N_6 π orbital of the thiazolo ring. It is surprising to notice a decrease in the population of the NBO C_1-C_2 , $C_{31}-C_{33}$, and $C_{10}-O_{23}$ reflecting a charge transfer away from the thiazolo[3,2-a]pyridine ring. In conclusion, 1 enjoys the linear conjugation that is responsible for the observed spectrum. No specific part of the molecule manifests itself in the observed spectrum.

Table 6. Second Order Perturbation Interaction Energy Values Computed in the NBO Basis for the studied compounds 1-4, calculated at B3LYP/6-311G (d, p).

Compound	Donor	Acceptor	E ⁽²⁾ (kcal/mol)	NBO	Population
1H	πC_1-C_2	$\pi^*C_{27}-N_{29}$	23.58	C_1-C_2	1.84983
	πC_9-C_{11}	$\pi^*C_{10}-O_{23}$	20.87	C_9-C_{11}	1.86448
	$\sigma C_{11}-H_{12}$	$\sigma^*S_8-C_9$	10.96	$C_{11}-H_{12}$	1.95503
	$\pi C_{32}-C_{34}$	$\pi^*C_{37}-C_{41}$	25.59	$C_{32}-C_{34}$	1.51731
	$\pi C_{35}-C_{39}$	$\pi^*C_{36}-C_{40}$	23.32	$C_{35}-C_{39}$	1.50209
	LP (1) N_6	$\pi^*C_4-C_5$	33.88	LP (1) N_6	1.61488
	LP (1) N_6	$\pi^*C_{10}-O_{23}$	50.05	LP (2) S_8	1.73751
	LP (2) S_8	$\pi^*C_4-C_5$	23.87	LP (1) O_{23}	1.97186
	LP (1) O_{23}	RY^*C_{10}	14.14	LP (2) O_{23}	1.84468
	LP (2) O_{23}	$\sigma^*N_6-C_{10}$	26.81	LP (1) N_{24}	1.74481
	LP (2) O_{23}	$\sigma^*C_9-C_{10}$	18.74	LP (1) N_{29}	1.96851

Compound	Donor	Acceptor	E ⁽²⁾ ^a (kcal/mol)	NBO	Population
2CH ₃	LP(1) N24	π^* C1-C2	51.82	C1-C2	0.35144
	LP(1) N29	π^* C27	16.62	C31-C33	0.42571
	π^* C1-C2	π^* C27-N29	19.00	C10-O23	0.31646
	π^* C9-C11	π^* C31-C33	55.78		
	π^* C10-O23	π^* C9-C11	47.61		
	π^* C47-C49	π^* C46-C48	17.10	C47-C49	1.76398
	LP (1) N6	π^* C10-O23	50.19	LP (2) S8	1.73776
	LP (2) S8	π^* C4-C5	23.83	LP (1)N6	1.61466
	LP (2)O23	σ^* N6-C10	26.74	LP(1) N24	1.74631
	LP(1) N24	π^* C1-C2	51.24	LP (2)O23	1.84501
3OCH ₃	π^* C1-C2	π^* C27-N29	18.97	C1-C2	0.35064
	π^* C9-C11	π^* C31-C33	56.61	C31-C33	0.42485
	π^* C10-O23	π^* C9-C11	47.32	C10-O23	0.31674
	σ^* C11-H12	σ^* S8-C9	11.02	C11-H12	1.95484
	LP (1) N6	π^* C4-C5	33.65	LP (1) N6	1.61455
	LP (1) N6	π^* C10-O23	50.36	LP (2) S8	1.73841
	LP (2) S8	π^* C4-C5	23.66	LP (1)N24	1.74787
	LP(1) N24	π^* C1-C2	50.97	LP (2)O54	1.83780
	LP (2)O54	σ^* C18-C20	31.04	C1-C2	0.34997
	π^* C1-C2	π^* C27-N29	19.03	C31-C33	0.42542
4Cl	π^* C9-C11	π^* C31-C33	58.44	C10-O23	0.31769
	π^* C10-O23	π^* C9-C11	47.88		
	π^* C9-C11	π^* C10-O22	21.20	C9-C11	1.86172
	π^* C46-C48	π^* C45-C47	17.17	C46-C48	1.76289
	LP (1) N6	π^* C4-C5	34.25	LP (1) N6	1.61550
	LP (1) N6	π^* C10-O22	49.64	LP (2) S8	1.73641
	LP (2) S8	π^* C4-C5	24.15	LP (1)N23	1.74175
	LP(1) N23	π^* C1-C2	52.68	LP (3)C154	1.92713
	LP (3)C154	π^* C16-C19	12.42	C1-C2	0.35469
	π^* C1-C2	π^* C26-N28	18.84	C30-C32	0.42716
	π^* C9-C11	π^* C30-C32	56.71	C10-O22	0.31575
	π^* C10-O22	π^* C9-C11	47.19	C16-C19	0.37962
	π^* C16-C19	π^* C13-C14	206.92	C13-C14	0.34433
	π^* C16-C19	π^* C15-C18	249.52	C15-C18	0.31072

^a E⁽²⁾ means energy of hyperconjugative interactions (stabilization energy).

LP_(n) is a valence lone pair orbital (n) on atom.

Table 7. Theoretical and experimental UV spectra of 1, calculated at CAM-B3LYP/6-311G (d, p).

state	TD-Theoretical							
	Gas phase				Xylene			
	Config uration	Coefficient	f	λ , nm	Configuration	Coefficient	f	λ , nm
I	125-126	0.694	0.412	403.8	125-126	0.692	0.494	414
	120-126	-0.15	0.115	310.7	123-126	-0.398	0.291	311
	123-126	0.626			124-126	0.468		
II	123-127	-0.16			124-127	0.215-		
	124-126	0.108			125-127	0.185-		
	124-127	-0.10						
	118-127	0.117	0.399	251.5	122-126	-0.267	0.952	256
	119-126	-0.25			123-127	0.363		
III	122-126	-0.14			123-128	-0.27		
	123-127	0.472			124-128	0.227-		
	123-128	0.17-			125-128	0.205-		
	124-128	-0.22			125-129	0.267		
	125-128	0.12-						
	125-129	0.100						

Table 7. Continued.

state	TD-Theoretical				Experimental	
	Acetone				Acetone	Xylene
	Configuration	Coefficient	f	λ , nm	λ_{nm}	λ_{nm}
I	125-126	0.692	0.471	412	415	418
	123-126	0.448				
II	124-126	-0.43	0.303	308	313	318
	124-127	0.209				
	125-127	0.137				

state	TD-Theoretical				Experimental	
	Acetone				Acetone	Xylene
	Configuration	Coefficient	f	λ , nm	λ_{nm}	λ_{nm}
III	119-126	0.331	0.542	257		
	119-127	0.117				
	122-126	0.225				
	123-127	0.244-				
	123-128	0.255				
	124-128	0.205				
	125-128	0.268				
	125-129	0.185-				

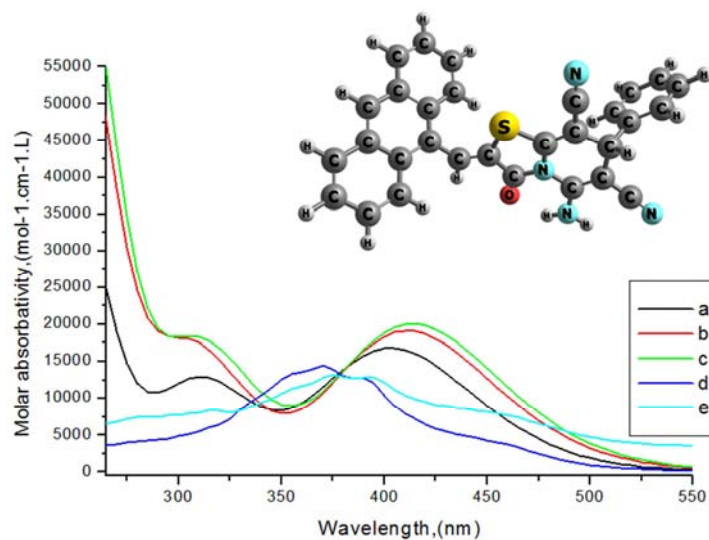


Figure 8. Electronic absorption spectra of 1, (a) theoretical in gas phase, (b) theoretical in acetone, (c) theoretical in xylene, (d) experimental in acetone, (e) experimental in xylene.

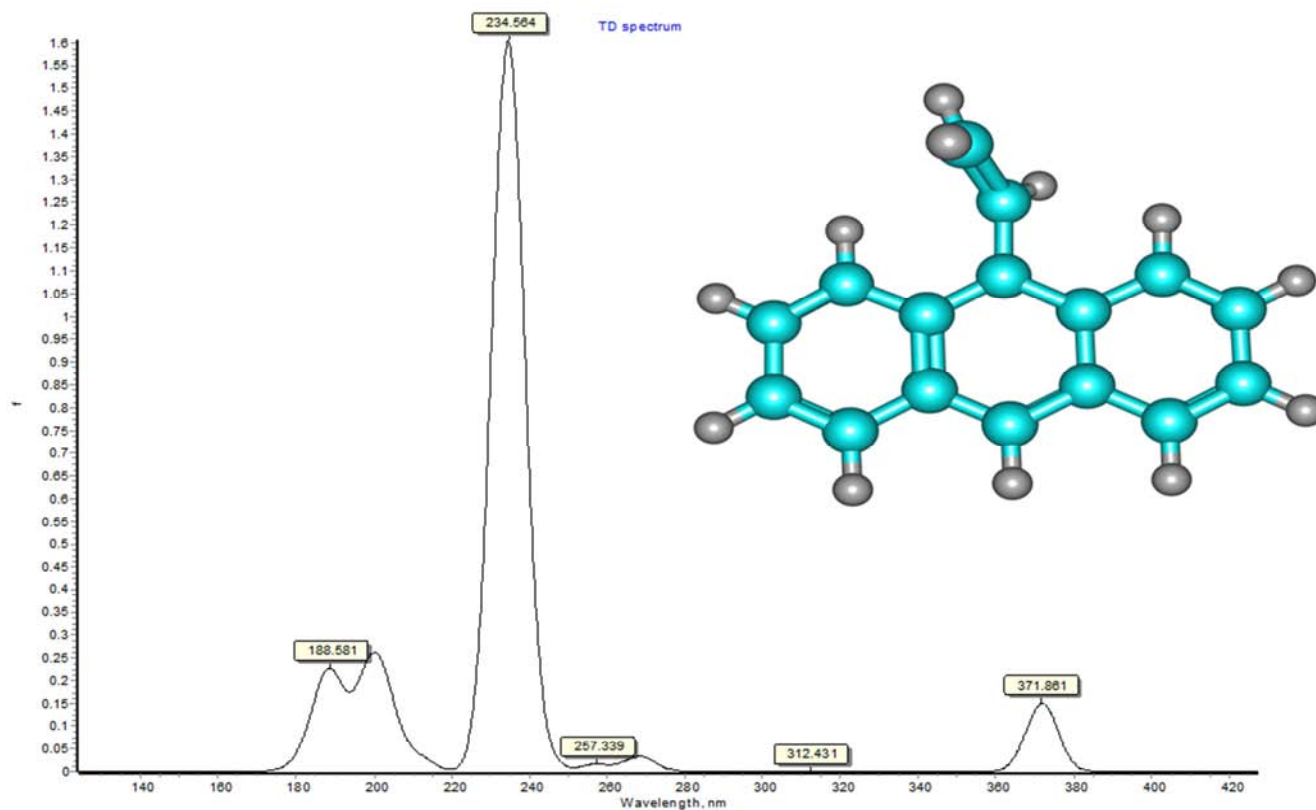


Figure 9. Theoretical transitions at TD-DFT B3LYP/6-311G (d, p) level of theory of (a) 9-vinylanthracene.

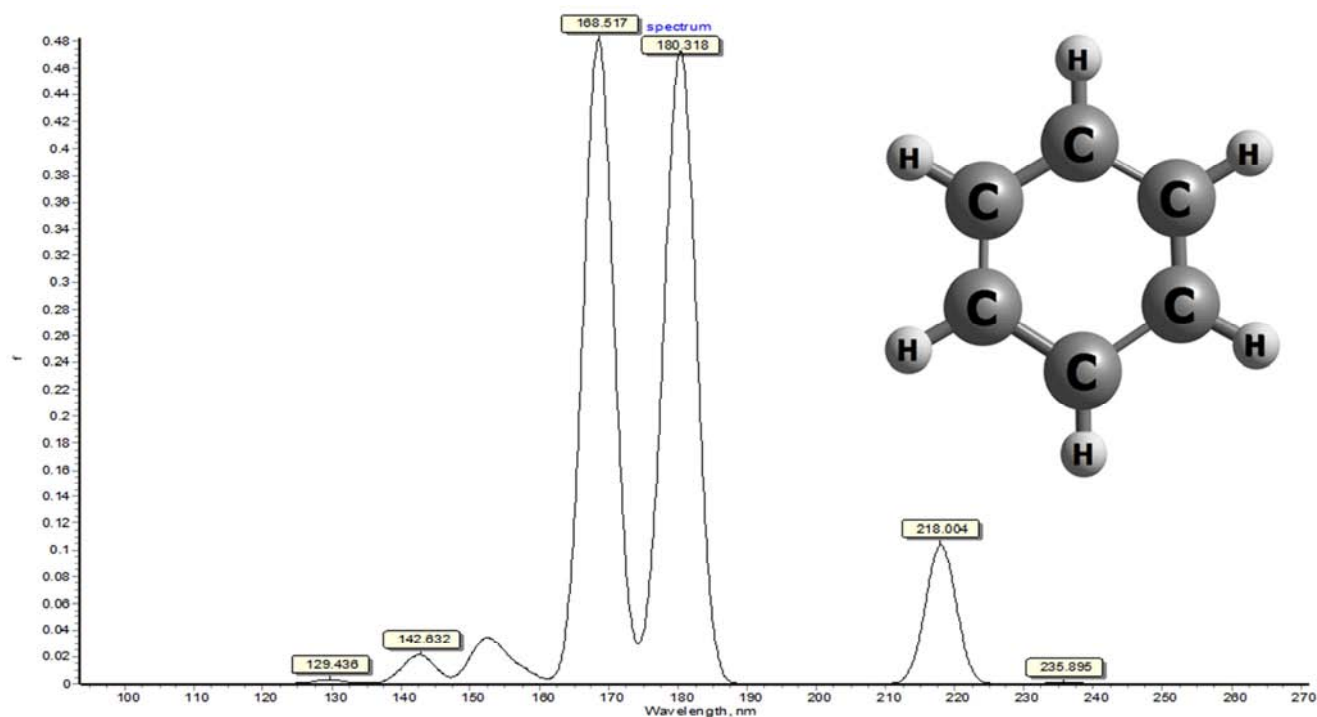


Figure 10. Theoretical transitions at TD-DFT B3LYP/6-311G (d, p) level of theory of (b) benzene.

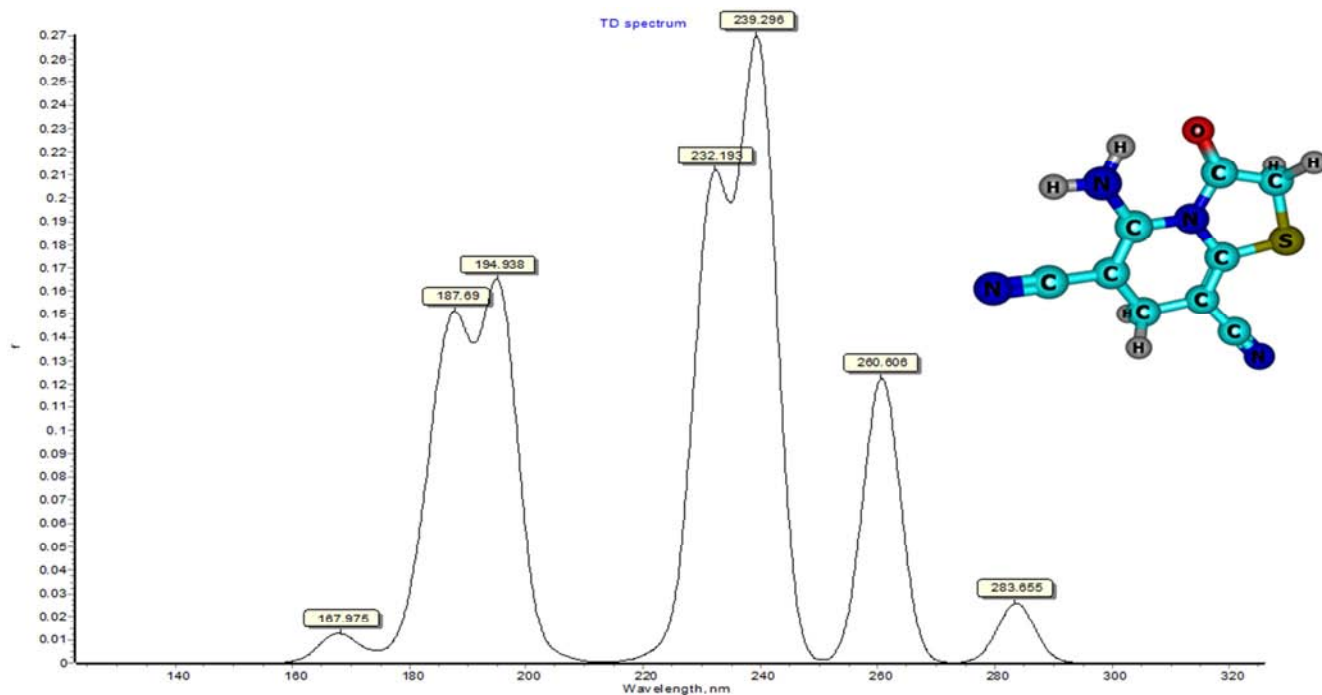


Figure 11. Theoretical transitions at TD-DFT B3LYP/6-311G (d, p) level of theory of (c) 5-amino-3-oxo-3,7-dihydro-2H-thiazolo[3,2-a]pyridine-6,8-dicarbonitrile.

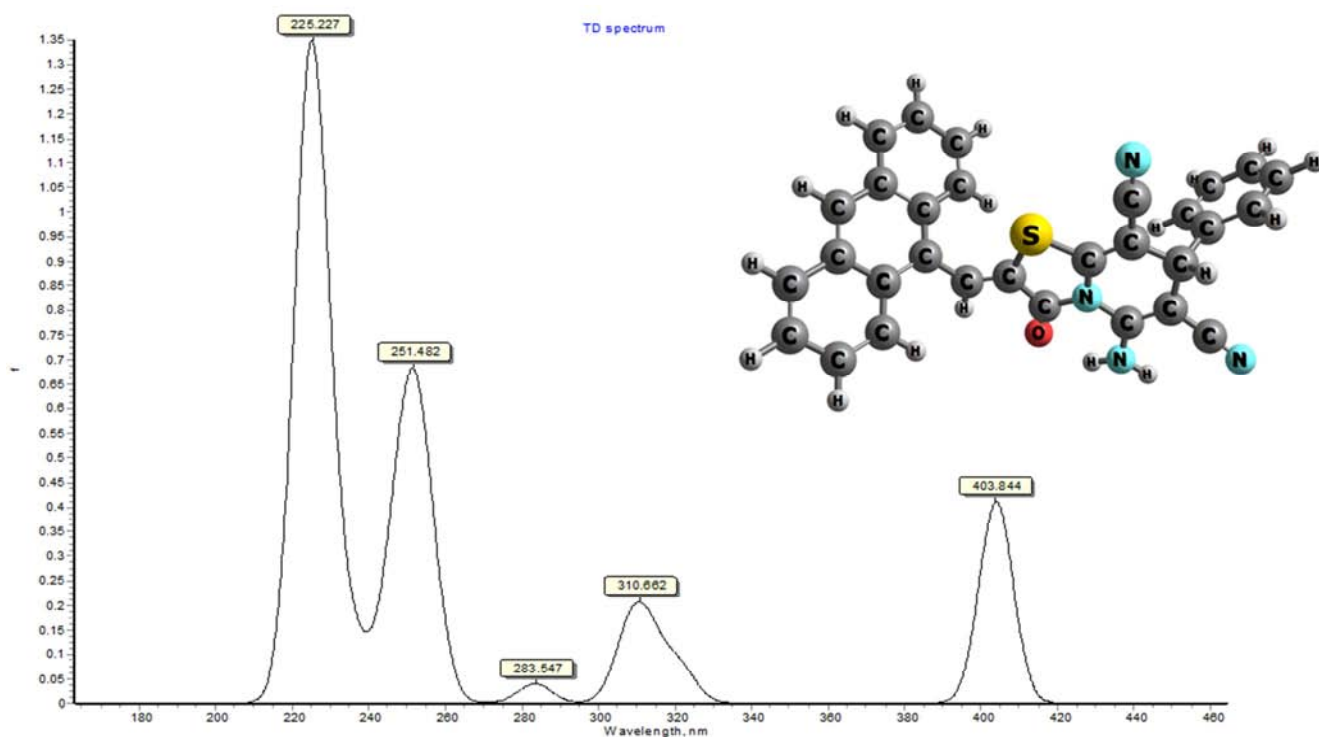
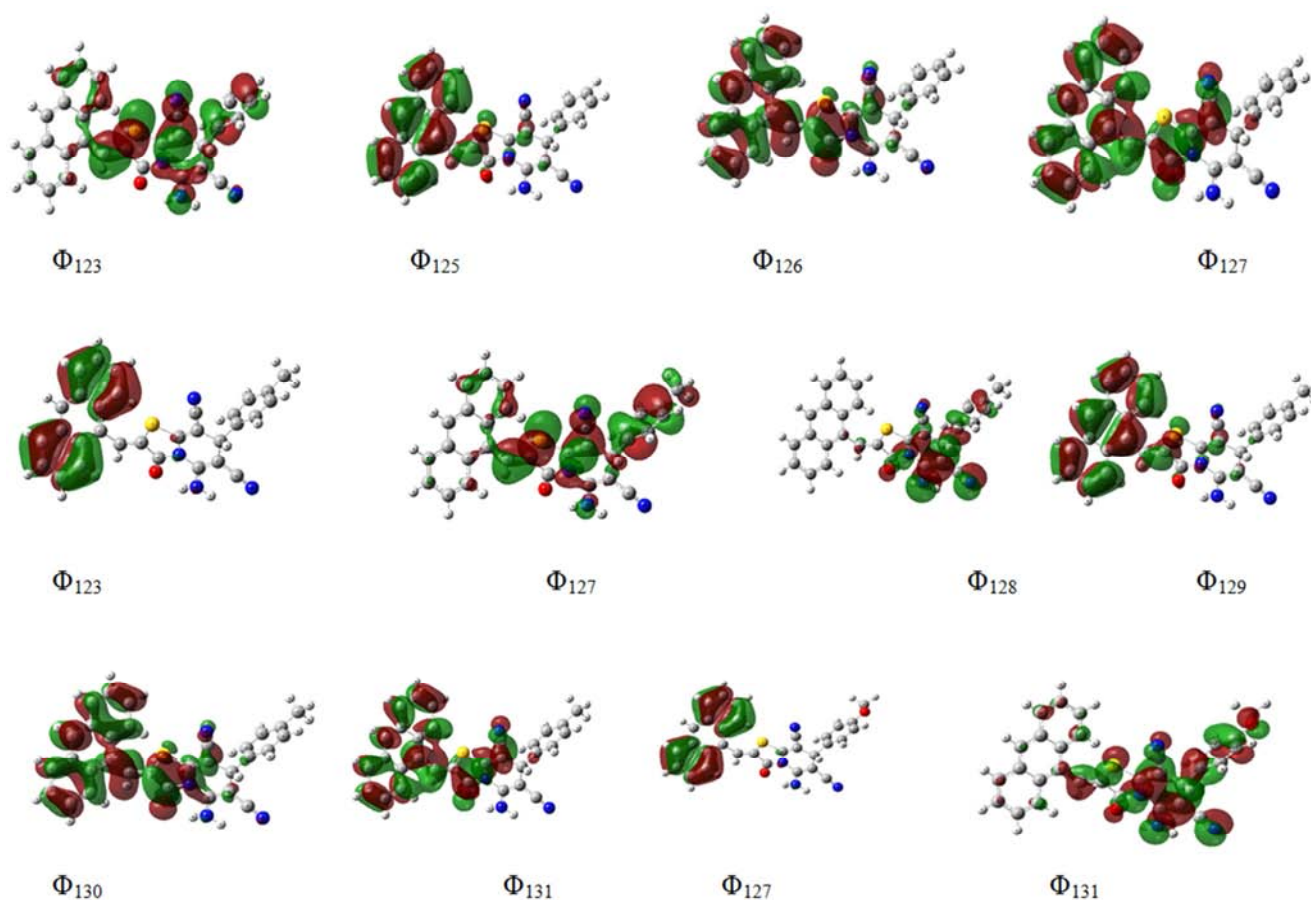


Figure 12. Theoretical transitions at TD-DFT B3LYP/6-311G (d, p) level of theory of compound 1 5-amino-2-(anthracen-9-ylmethylene)-3-oxo-7-phenyl-2,3-dihydro-7H thiazolo[3,2-a]pyridine-6,8-dicarbonitrile.



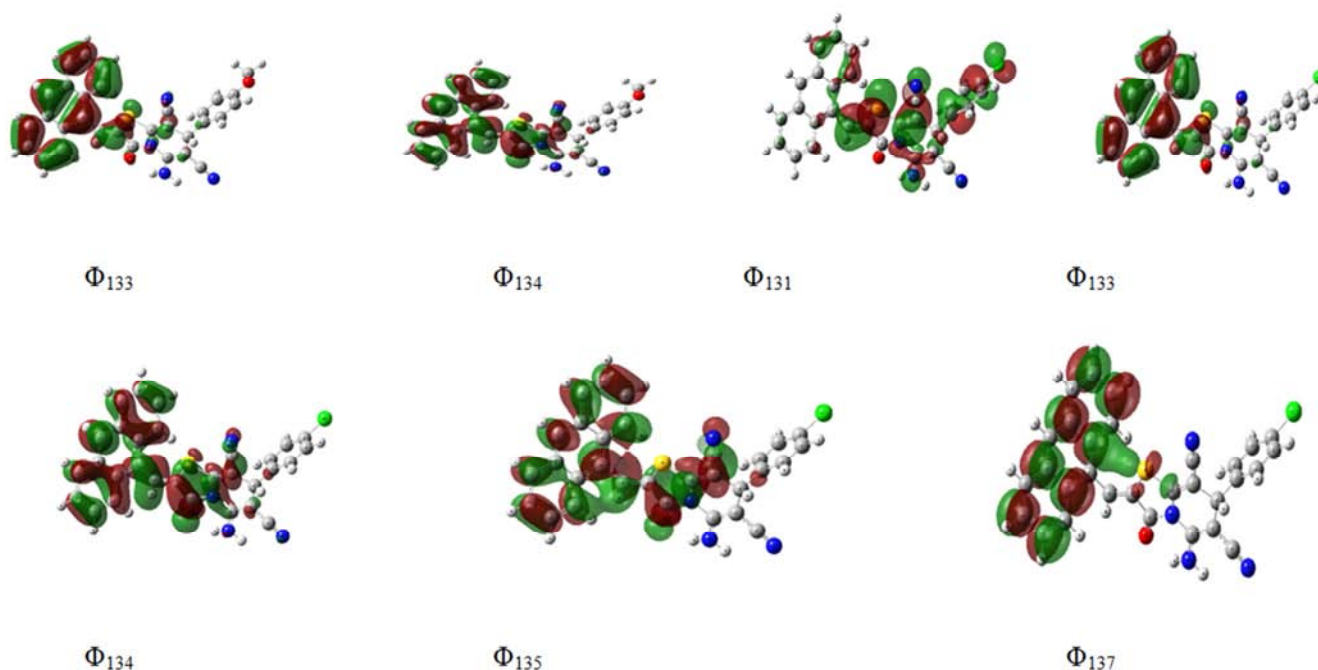


Figure 13. Electron density contours of the studied compounds 1-4.

3.5.2. Electronic Absorption Spectra of Compound 2

Compound 2 results when our insertion of CH₃ group in position X of Ph-X in compound 1. "Figure 14", and Table 8 elucidate the experimental and theoretical electronic absorption spectra of compound 2 in two solvents xylene and acetone. In non-polar solvent (xylene), the experimental spectrum is composed of two bands, at 417 nm, and 315 nm. The blue shift of the two bands, results from increasing solvent polarity from xylene to acetone where the first band is shifted to 414 nm, and the second band is shifted to 313 nm, respectively. Furthermore, The two observed bands are assigned as (π - π^*) transitions, based on the values of molar absorptive ($\epsilon = 50000$), due to, increasing solvent polarity causes a marked increase in the intensity of both bands. CAM / B3LYP/6-311G (d, p) level used for the interpretation of the experimentally observed UV Spectra of 2 in non-polar solvent (xylene) and polar-solvent (acetone) these requires the theoretical calculations of the vertical transitions. State (I) the non-polar solvent (xylene), shows the spectrum band experimentally at 417 nm is reproduced theoretically at 414 nm (state I), as shown in Table 8, which involves orbital's ϕ_{129} and ϕ_{130} , showing a good agreement between the observed wavelength with the calculated wavelength. The gas phase computed theoretically give a vertical excitation at 403 nm (state I). Increasing solvent polarity results in a blue shift of λ_{\max} of this band to 414 nm. The polar solvent (acetone) appeared theoretically band at 410 nm (state I). The second band observed experimentally in xylene at 315 nm, is reproduced theoretically at 311 nm (state II), indicating that the orbital's ϕ_{128} and ϕ_{130} are involved in this transition. Theoretical gas

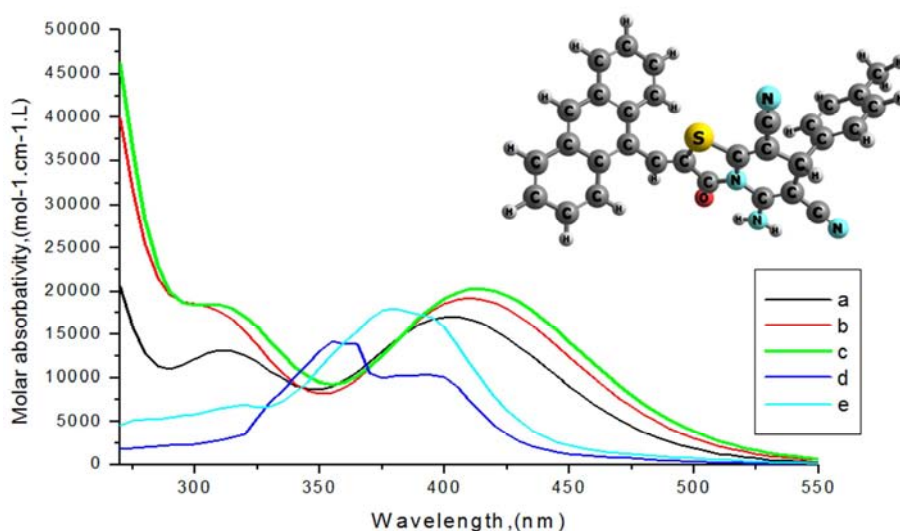
phase calculations give a wavelength at 309 nm (state II). This same band is observed at 313 nm in acetone, where theoretical calculations in acetone reproduces this band at 307 nm (state II), which is lower than the observed wavelength, where the orbital's ϕ_{127} and ϕ_{130} are involved in this transition. The third band theoretically in xylene at 257 nm, (state III), indicating that the orbital's ϕ_{127} and ϕ_{131} are involved in this transition. Theoretical gas phase calculations give a wavelength at 253 nm (state III), this same band theoretical calculations in acetone at 256 nm (state III), where the orbital's ϕ_{123} and ϕ_{130} are involved in this transition. The six orbital's ϕ_{123} , ϕ_{127} , ϕ_{128} , ϕ_{129} , ϕ_{130} and ϕ_{131} involved in the theoretical transitions of 2, are shown in "Figure 13". The first band which involves ϕ_{129} and ϕ_{130} has electron density delocalization, while orbital's ϕ_{123} , ϕ_{127} , ϕ_{128} and ϕ_{131} have a Charge Transfer CT character. The results of NBO analysis of compound 2 tabulated in Table 6 indicate that there is a strong hyper conjugative interactions $\pi^*C_9-C_{11} \rightarrow \pi^*C_{31}-C_{33}$, LP (1) $N_{24} \rightarrow \pi^*C_1-C_2$, LP (1) $N_6 \rightarrow \pi^*C_{10}-O_{23}$, $\pi^*C_{10}-O_{23} \rightarrow \pi^*C_9-C_{11}$, LP (2) $O_{23} \rightarrow \sigma^*N_6-C_{10}$, LP (2) $S_8 \rightarrow \pi^*C_4-C_5$, and $\pi^*C_1-C_2 \rightarrow \pi^*C_{27}-N_{29}$, for 2 is 56.16, 51.24, 50.19, 47.32, 26.74, 23.83 and 18.97 kcal/mol, respectively. NBO analysis of the p-CH₃ derivative Table 6 indicates that it retained the extended conjugation of 1 as revealed by the interaction of C-N NBOs with those of pyridine ring. Furthermore, the interaction of the nitrogen lone orbital's with the C10-O23, and C1-C2 π^* orbital is marked. The population of the NBO C1-C2, C31-C33, and C10-O23 reflecting a charge transfer away from the thiazolo[3,2-a]pyridine ring. This is also evident in the case of the population of the nitrogen lone orbital LP (1) N6.

Table 8. Theoretical and experimental UV spectra of **2**, calculated at CAM-B3LYP/6-311G (d, p).

state	TD-Theoretical							
	Gas phase				Xylene			
	Config uration	Coefficient	f	λ , nm	Config uration	Coefficient	f	λ , nm
I	129-130	0.694	0.418	403	129-130	0.692	0.500	414
	124-130	-0.10	0.136	309	126-130	-0.113	0.288	311
	126-130	0.265			127-130	-0.416		
II	127-130	0.585			128-130	0.433		
	127-131	0.15-			128-131	0.204		
					129-131	0.199		
III	122-131	0.11-	0.376	253	123-130	0.183	0.976	257
	123-130	-0.34			125-130	0.282		
	125-130	-0.14			126-131	0.105		
	126-131	0.131			127-131	0.314		
	127-131	0.410			127-132	0.257-		
	127-132	-0.17			128-132	-0.230		
	128-132	0.22-			129-132	-0.190		
	129-132	0.11-			129-133	0.263		

Table 8. Continued.

state	TD-Theoretical				Experimental	
	Acetone				Acetone	Xylene
	Configuration	Coefficient	f	λ , nm	λ_{nm}	λ_{nm}
I	129-130	0.692	0.473	410	414	417
	125-130	0.145-				
	127-130	0.468				
II	127-131	0.114				
	128-130	0.389-	0.305	307	313	315
	128-131	0.193-				
	129-131	0.147-				
	123-130	0.401				
	123-131	-0.136				
III	126-130	0.225				
	127-131	0.198	0.541	256		
	127-132	0.226-				
	128-132	-0.190				
	129-132	-0.225				
	129-133	0.191				

**Figure 14.** Electronic absorption spectra of **2**, (a) theoretical in gas phase, (b) theoretical in acetone, (c) theoretical in xylene, (d) experimental in acetone, (e) experimental in xylene.

3.5.3. Electronic Absorption Spectra of Compound 3

To complete our investigation of substituent effect on the

electronic structure and spectra of compound **1**, we introduce OCH₃-group in position X in Ph-X of compound **1** gives compound **3**. The experimental and theoretical electronic

absorption spectra of compound 3 in xylene and acetone are shown in "Figure 15", and Table 9. The experimental spectrum in xylene is composed of two bands at 419 nm, and 316 nm. The change of solvent polarity from xylene to acetone results in a blue shift of the two bands, where the first band is shifted to 416 nm, and the second band is shifted to 313 nm, respectively. Furthermore, increasing solvent polarity causes a marked increase in the intensity of both bands. The values of molar absorptivity ($\epsilon = 45000$) indicates that the two observed bands have $\pi-\pi^*$ character. The theoretical vertical transitions using CAM / B3LYP / 6-311G (d, p) level is valuable for the analysis of the experimental UV Spectra of 3 in xylene and acetone, which gives values for λ_{max} of 415 nm (state I) for the first band, 311 nm (state II) for the second band, 258 nm (state III) for the third band, as shown in Table 9. Theoretical transitions in the gas phase give a vertical excitation at 404 nm (state I), which is about 15 nm lower than the experimental wavelength, where it involves the same orbitals as in xylene. Theoretical vertical excitation calculations in acetone give λ_{max} of this band at 411 nm (state I), which shows a fair agreement, implying that the orbitals involved in this transition are ϕ_{133} and ϕ_{134} . The experimental second band observed at 316 nm in xylene, is reproduced theoretically at 311 nm (state II), where the calculations in xylene indicate that the orbital's ϕ_{131} and ϕ_{134} are involved in this transition. Gas phase calculations give λ_{max} at 311 nm (state II). Theoretical calculations in acetone

show that, this band appears at 308 nm (state II), which is lower than the experimental wavelength. The third state ($\pi-\pi^*$)¹, theoretically at 258 nm in xylene, (state III), where the calculations in xylene indicate that the orbital's ϕ_{127} and ϕ_{134} are involved in this transition. Gas phase calculations give λ_{max} at 258 nm (state III). Theoretical calculations in acetone show that, this band appears at 253 nm (state III). The four orbital's ϕ_{127} , ϕ_{131} , ϕ_{133} and ϕ_{134} involved in the theoretical transitions of 3, are shown in "Figure 13". where the first band which involves ϕ_{133} and ϕ_{134} , show a CT character, while orbital's ϕ_{131} and ϕ_{134} & ϕ_{127} and ϕ_{134} involved in the second, and third bands show electron density delocalization and also a CT character. The results of NBO analysis of compound 3 tabulated in Table 6 indicate that there is a strong hyper conjugative interactions $\pi^*C_9-C_{11} \rightarrow \pi^*C_{31}-C_{33}$, LP (1) $N_{24} \rightarrow \pi^*C_1-C_2$, LP (1) $N_6 \rightarrow \pi^*C_{10}-O_{23}$, $\pi^*C_{10}-O_{23} \rightarrow \pi^*C_9-C_{11}$, LP (1) $N_6 \rightarrow \pi^*C_4-C_5$, LP (2) $O_{54} \rightarrow \sigma^*C_{18}-C_{20}$ and LP (2) $S_8 \rightarrow \pi^*C_4-C_5$, for 3 is 58.44, 50.97, 50.36, 47.88, 33.65, 31.04 and 23.66 kcal/mol, respectively. NBO analysis of the p-OCH₃ derivative Table 6 indicates that it retained the extended conjugation of 1 as revealed by the interaction of C–N NBOs with those of pyridine ring. Furthermore, the interaction of the oxygen lone orbital's with the C18–C20 σ^* orbital is marked. The population of the NBO C1–C2, C31–C33, and C10–O23 reflecting a charge transfer away from the thiazolo[3,2-a]pyridine ring.

Table 9. Theoretical and experimental UV spectra of 3, calculated at CAM-B3LYP/6-311G (d, p).

state	TD-Theoretical							
	Gas phase				Xylene			
	Config uration	Coefficient	f	λ , nm	Config uration	Coefficient	f	λ , nm
I	133-134	0.694	0.425	404	133-134	0.692	0.508	415
	130-134	0.407	0.193	311	130-134	0.357	0.284	311
II	131-134	0.473			131-134	0.504		
	131-135	0.145			131-135	0.175		
	133-135	0.222			133-135	0.223		
	127-134	0.313	0.286	258	127-134	0.486	0.568	258
	130-135	-0.31			127-135	0.157-		
	130-136	0.109			129-134	0.285		
III	131-135	0.21-			132-136	0.177		
	132-134	0.191			133-136	0.113-		
	132-135	-0.21			133-137	0.25		
	132-136	0.321						
	133-136	-0.11						

Table 9. Continue.

state	TD-Theoretical				Experimental	
	Acetone				Acetone	Xylene
	Configuration	Coefficient	f	λ , nm	λ_{nm}	λ_{nm}
I	133-134	0.692	0.480	411	416	419
	130-134	0.358	0.301	308		
II	131-134	0.520				
	131-135	0.179			313	316
	133-135	0.162				
	127-134	-0.261	0.534	253		
	129-134	0.372				
III	130-139	0.157				
	131-139	0.139				
	133-137	0.41				

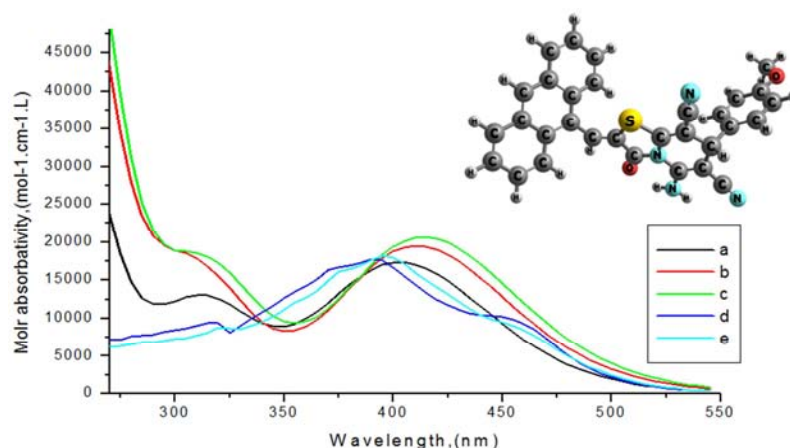


Figure 15. Electronic absorption spectra of 3, (a) theoretical in gas phase, (b) theoretical in acetone, (c) theoretical in xylene, (d) experimental in acetone, (e) experimental in xylene.

3.5.4. Electronic Absorption Spectra of Compound 4

Compound 4 results by inserting Cl-atom in position X in Ph-X of compound 1. The experimental and theoretical electronic absorption spectra of compound 4 in xylene and acetone are shown in "Figure 16", and Table 10. The experimental spectrum in xylene is composed of two bands at 420 nm, and 314 nm. The change of solvent polarity from xylene to acetone results in a small red shift by 3 nm of the first band, and the second band red shift by 4 nm. Additionally, increasing solvent polarity causes a marked decrease in the intensity of both bands. The values of molar absorptivity ($\epsilon = 45000$) indicates that the two observed bands have $\pi-\pi^*$ character. The theoretical vertical transitions using CAM / B3LYP/6-311G (d, p) level is valuable for the analysis of the experimental UV Spectra of 4 in xylene and acetone, which gives values for λ_{\max} of 419 nm (state I) for the first band, 311 nm (state II) for the second band, and 258 nm (state III) for the third band as shown in Table 10. The theoretical transition of the first band in xylene involves orbital's ϕ_{133} and ϕ_{134} , showing a good agreement between the observed and the calculated wavelengths. Theoretical transitions in the gas phase give a vertical excitation at 407 nm (state I), which is about 13 nm lower than the experimental wavelength, where it involves the same orbitals as in xylene. Theoretical vertical excitation calculations in acetone give λ_{\max} of this band at 415 nm (state I), which shows a fair agreement, implying that the orbitals involved in this transition are ϕ_{133} and ϕ_{134} . The experimental second band observed at 314 nm in xylene, is reproduced theoretically at 311 nm (state II), where the calculations in xylene indicate that the orbital's ϕ_{131} and ϕ_{134} are involved in this transition. Gas phase calculations give λ_{\max} at

311 nm (state II). Theoretical calculations in acetone show that, this band appears at 308 nm (state II), which is lower than the experimental wavelength. Theoretical gas phase wavelength is found to be lower than the observed wavelength in acetone. The third state ($\pi-\pi^*$)¹, which theoretically at 258 nm in xylene, (state III), where the calculations in xylene indicate that the orbital's ϕ_{131} and ϕ_{135} are involved in this transition. Gas phase calculations give λ_{\max} at 253 nm (state III). Theoretical calculations in acetone show that, this band appears at 254 nm (state III). It shows that the orbitals involved in the transition are ϕ_{133} and ϕ_{137} . The five orbital's ϕ_{131} , ϕ_{133} , ϕ_{134} , ϕ_{135} and ϕ_{137} involved in the theoretical transitions of 4, are shown in "Figure 13", where the first band which involves ϕ_{133} and ϕ_{134} , show a CT character, while orbital's ϕ_{131} and ϕ_{135} & ϕ_{131} and ϕ_{134} & ϕ_{133} and ϕ_{137} involved in the second and third bands show electron density delocalization and also CT character. The results of NBO analysis of compound 4 tabulated in Table 6 indicate that there is a strong hyper conjugative interactions $\pi^*C_{16}-C_{19} \rightarrow \pi^*C_{15}-C_{18}$, $\pi^*C_9-C_{11} \rightarrow \pi^*C_{30}-C_{32}$, LP (1) $N_{23} \rightarrow \pi^*C_1-C_2$, LP (1) $N_6 \rightarrow \pi^*C_{10}-O_{22}$, $\pi^*C_{10}-O_{22} \rightarrow \pi^*C_9-C_{11}$, LP (1) $N_6 \rightarrow \pi^*C_4-C_5$ and LP (2) $S_8 \rightarrow \pi^*C_4-C_5$, for 4 is 249.52, 56.71, 52.68, 49.64, 47.19, 34.25, and 24.15 kcal/mol, respectively. NBO analysis of the p-Cl derivative Table 6 indicates that it retained the extended conjugation of 1 as revealed by the interaction of C-Cl NBOs with those of phenyl ring. Furthermore, the interaction of the chlor lone orbital's with the C30-C32 σ^* orbital is marked. The population of the NBO C15-C18, C10-O22, C13-C14, C1-C2, C16-C19, and C30-C32 reflecting a charge transfer away from the thiazolo[3,2-a]pyridine ring.

Table 10. Theoretical and experimental UV spectra of 4, calculated at CAM-B3LYP/6-311G (d, p).

state	TD-Theoretical							
	Gas phase				Xylene			
	Config uration	Coefficient	f	λ , nm	Config uration	Coefficient	f	λ , nm
I	133-134	0.694	0.420	407	133-134	0.692	0.509	419
	131-134	-0.24	0.165	311	129-134	0.120	0.323	311
	132-134	0.569			131-134	0.468		
II	132-135	0.267			132-134	0.406		
	133-135	0.150			132-135	0.176		
					133-135	-0.167		

state	TD-Theoretical							
	Gas phase				Xylene			
	Config uration	Coefficient	f	λ , nm	Config uration	Coefficient	f	λ , nm
III	126-135	0.10-	0.521	253	130-134	0.227	0.869	258
	127-134	0.144			131-135	0.335		
	129-134	-0.160			131-136	-0.287		
	130-135	0.132			132-136	0.252-		
	131-135	0.415			133-136	0.268-		
	131-136	-0.250			133-137	0.229		
	132-136	0.25-						
	133-136	0.21-						
	133-137	0.126						

Table 10. Continued.

state	TD-Theoretical					Experimental	
	Acetone					Acetone	Xylene
	Configuration	Coefficient	f	λ , nm		λ_{nm}	λ_{nm}
I	133-134	0.692	0.483	415		423	420
	129-134	0.103					
	131-134	0.485					
II	131-135	0.103	0.539	254		318	314
	132-134	-0.389					
	132-135	-0.188					
	133-135	-0.133					
	128-134	0.256-					
	130-134	0.383					
III	130-135	0.112	0.414				
	131-140	0.167-					
	133-136	-0.138					
	133-137	0.414					

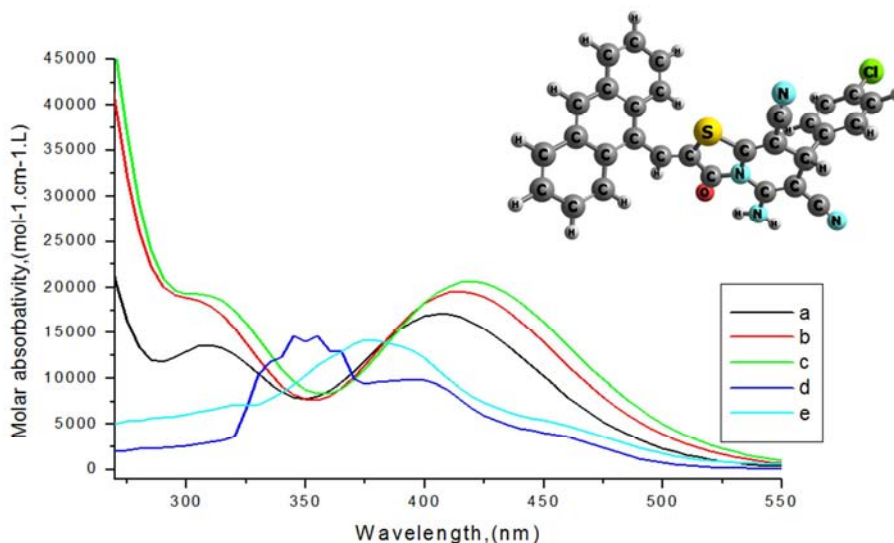


Figure 16. Electronic absorption spectra of 4, (a) theoretical in gas phase, (b) theoretical in acetone, (c) theoretical in xylene, (d) experimental in acetone, (e) experimental in xylene.

3.6. Summary and Conclusion

The optimized electronic structure of 5-amino-2-(anthracen-9-ylmethylene)-3-oxo-7-phenyl-2,3-dihydro-7H-thiazolo[3,2-a]pyridine-6,8-dicarbonitrile, compound 1 and its derivatives, 2–4, are investigated theoretically at B3LYP/6-311G (d, p). All the studied compounds are found to be non-planar. The dihedral angles results show that the phenyl at C₃ and the anthranyl at C₉ are out of the molecular plane of thiazolo[3,2-a]pyridines by 111° and 128° respectively, resulting in a significant impact on

the electronic and structural properties of compounds 1–4. The ground state properties of 1 and its derivatives show that compound 4 has the lowest E_{HOMO} , E_{LUMO} , and E_{gap} indicating highest reactivity. From the computed dipole moment, compound 3 is found to have the highest polarity. The HOMO-LUMO energy gap helped in analyzing the chemical reactivity, hardness, softness, chemical potential and electro negativity. The natural charge distribution of the compounds 1–4 were studied. The non-linear optical indicating from the values of calculated dipole moment and first order hyperpolarizability.

The total electron density surface with MEP confirmed the different negative and positive potential sites of the molecule. Electronic absorption spectra are investigated experimentally in non-polar solvent (xylene) and polar solvent (acetone); and theoretically in gas phase, xylene and acetone using CAM-B3LYP/6-311G (d, p). The band maxima (λ_{max}) and intensities of the spectra are found to have solvent dependence. The bands of compounds 1, 2, and 3 show blue shift, while compounds 4 show red shift. Theoretical calculations of the vertical excitations at the CAM-B3LYP/6-311G (d, p) reproduce the experimental spectra, indicating a good agreement between theory and experiment. The NBO analysis of the compounds 1–4 indicated the intermolecular charge transfer between the bonding and antibonding orbital's.

References

- [1] Hari Datta Khanal and Yong Rok Lee, (2015) Organocatalyzed oxidative N-annulation for diverse and polyfunctionalized pyridines. *Chem. Commun.* 51: 9467-9470. doi: 10.1039/c5cc01807b.
- [2] Yepes AF, Jaimes E, Bahsas A, Palma A, Hursthouse MB, Cobo J, Glidewell C. (2010) Ring conformations and intermolecular interactions in two fused dibenzoazocines. *Acta Crystallographica. Section C, Crystal Structure Communications.* 66: 284-288. doi: 10.1107/S0108270110014708.
- [3] Suksrichavalit T., Prachayasittikul S., Nantasenamat C., Isarankura-Na-Ayudhya V., Prachayasittikul C., (2009) Copper complexes of pyridine derivatives with superoxide scavenging and antimicrobial activities. *Eur. J. Med. Chem.* 44: 3259-3265. doi: 10.1016/j.ejmech.2009.03.033
- [4] Mohamed Ibrahim H., Haider Behbehani, (2014) Synthesis of A New Class of Pyridazin-3-one and 2-Amino-5-arylazopyridine Derivatives and Their Utility in the Synthesis of Fused Azines. *Mol.* 19: 2637-2654. doi: 10.3390/molecules19022637.
- [5] Roxana M. Butnariu, Maria D. Caprosu, Vasilichia Bejan, Ionel I. Mangalagiu, Margareta Ungureanu, Antonia Poiata, Cristina Tuchilus, Margareta Florescu, (2009) Pyridazine and phthalazine derivatives with potential antimicrobial activity. *J. Hetero. Chem.* 44: 1149-1152. <https://doi.org/10.1002/jhet.5570440528>
- [6] Roberta Barbaro, Laura Betti, Maurizio Botta, Federico Corelli, Gino Giannaccini, Laura Maccari, Fabrizio Manetti, Giovannella Strappaghetti, and Stefano Corsano, (2001) Synthesis, Biological Evaluation, and Pharmacophore Generation of New Pyridazinone Derivatives with Affinity toward $\alpha 1$ - and $\alpha 2$ -Adrenoceptors. *J. Med. Chem.* 44: 2118-2132. doi: 10.1021/jm010821u.
- [7] Tracy E, Zhu M, Streiff C, Sahn DJ, Ashraf M. (2018) Quantification of the area and shunt volume of multiple, circular, and noncircular ventricular septal defects: A 2D/3D echocardiography comparison and real time 3D color Doppler feasibility determination study. *Echocardiography.* 35: 90-99. doi: 10.1111/echo.13742.
- [8] Nermin A. Marzouk, Ahmed H. Shamroukh, Abeer H. Al-Saadny, J. A. Micky and Farouk, M. E. Abd El-Megeid, (2011) Synthesis, Isomerization, and Antimicrobial Evaluation of Some IndenothienoPyrimidine Derivatives. *J. Amer. Sci.* 7: 362-369.
- [9] Houda Serrar, et al, (2018) Two derivatives of 7-amino-thiazolo[3,2-a]pyrimidine as inhibitors of mild steel corrosion in 1.0M HCl solution: part I synthesis of inhibitors and electrochemical study. *J. Chem. Tech. Meta.* 53: 324-335.
- [10] Mohamoud N. A., (2015) Synthesis of some new thiazolo, pyrano and pyrimidinone derivatives of expected biological activities. *Int. J. Adv. Res.* 3: 977-987.
- [11] Hany J. Al-Majjar, Assem Barakar, Abdullah M. Al-Majid, Yahia, N. Mabkhot, Manuel Weber, Hazem, A. Ghabbour, Hoongkun Fun, (2014) A Greener, Efficient Approach to Michael Addition of Barbituric Acid to Nitroalkene in Aqueous Diethylamine Medium. *Mol.* 19: 1150-1162. doi:10.3390/molecules19011150
- [12] Affram K. et al, (2015) In Vitro and in Vivo Antitumor Activity of Gemcitabine Loaded Thermosensitive Liposomal Nanoparticles and Mild Hyperthermia in Pancreatic Cancer. *Int. J. Adv. Res.* 3: 859-874.
- [13] Teuber L., (1990) Naturally Occurring 1,2-Dithiolanes and 1,2,3-Trithianes. Chemical and Biological Properties. *J. Sulfur Reports.* 9: 257-333. <https://doi.org/10.1080/01961779008048732>
- [14] Minotti Menna P G, Salvatorelli E, Cairo G, Gianni L., (2004) LAnthracyclines: molecular advances and pharmacologic developments in antitumor activity and cardiotoxicity. *Pharmacol Rev.* 56: 185-229. doi: 10.1124/pr.56.2.6
- [15] Kanda N. et al., (1971) A new antitumor antibiotic, kidamycin. I. Isolation, purification and properties of kidamycin. *J. Antibiotics,* 24: 599-606. <http://doi.org/10.7164/antibiotics.24.599>
- [16] Degtev MI., Dudukalov NV., (2012) Synthesis of new derivatives of 2-acylisothiocyanate of 1-nitro-9,10-anthraquinone with antimicrobial activity basic research, 3: 167-172.
- [17] Sendel E., – S (1964) Catalog of Copyright Entries: Third series. 172.
- [18] Ayres G. H., (1949), Evaluation of Accuracy in Photometric Analysis. *Anal. Chem.* 21: 652-657. doi: 10.1021/ac60030a002
- [19] Denisov Popov VY, (2008) Synthesis of new cationic monomers based on ω -bromocarboxylic acids CIO. Proceedings of the Conference "Modern high technologies" 4–C. 138.
- [20] Murata N, Allakhverdiev S. I, Nishiyama Y, (2012) The mechanism of photoinhibition in vivo: Re-evaluation of the roles of catalase, α -tocopherol, non-photochemical quenching, and electron transport. *Biochimica et Biophysica Acta (BBA)-Bioenergetics.* 1817: 1127-1133. <https://doi.org/10.1016/j.bbabi.2012.02.020>
- [21] Zvarych V. I., Musyanovych R. Ya., Chervetsova V. G., Komarovska-Porokhnyavets O. Z., Stasevych M. V., Novikov V. P., (2013) Synthesis of new derivatives of 2-acylisothiocyanate of 1-nitro-9, 10-anthraquinone with antimicrobial activity. *Academic Journals and Conferenes of Lviv Polytechnic National University. SCHMT* 761.

- [22] Abdel Halim S, Ali Kh. Khalil (2017) TD-DFT calculations, NBO analysis and electronic absorption spectra of some thiazolo[3,2-a]pyridine derivatives. *J. Mol. Struct.* 1147: 651-667. <http://dx.doi.org/10.1016/j.molstruc.2017.06.098>.
- [23] Abdel Halim S, Ibrahim MA (2017) Synthesis, DFT calculations, electronic structure, electronic absorption spectra, natural bond orbital (NBO) and nonlinear optical (NLO) analysis of the novel 5-methyl-8H-benzo[h]chromeno[2,3-b][1,6]naphthyridine-6(5H),8-dione (MBCND). *J. Mol. Struct.* 1130: 543-558. <http://dx.doi.org/10.1016/j.molstruc.2016.10.058>.
- [24] Abdel Halim S, Laila I. Ali, Sameh Gamal Sanad (2017) Theoretical calculations of solvation 12-Crown-4 (12CN4) in aqueous solution and its experimental interaction with nano CuSO₄. *Int. J. Nano Dimens.*, 8: 142-158. DOI: 10.22034/ijnd.2017.24995.
- [25] Becke AD (1993) A new mixing of Hartree-Fock and local density-functional theories. *J. Chem. Phys.* 98: 1372-1376. doi: 10.1063/1.464304. Becke AD (1993) Densityfunctional thermochemistry, III: The role of exact exchange. *J. Chem. Phys.* 98: 5648-5652. doi: 10.1063/1.464913
- [26] Lee C, Yang W, Parr RG (1988) Development of the Colle-Salvetti correlation-energy formula into a functional of the electron density. *Phys. Rev. B Condens. Matter.* 37: 785-789. doi:10.1103/PhysRevB.37.78.
- [27] Stefanov B, B. G. Liu, A. Liashenko, P. Piskorz, I. Komaromi, R. L. Martin, D. J. Fox, T. Keith, M. A. Al-Laham, C. Y. Peng, A. Nanayakkara, M. Challacombe, P. M. W. Gill, B. Johnson, W. Chen, M. W. Wong, C. Gonzalez, J. A. Pople, Gaussian, Inc., Pittsburgh PA. (2003).
- [28] Frisch M, J. G. W. Trucks, H. B. Schlegel, G. E. Scuseria, et al., Gaussian, Inc., Wallingford CT, (2009).
- [29] GaussView, Version 5, Dennington, R.; Keith, T.; Millam, J. Semichem Inc., Shawnee Mission KS, (2009).
- [30] <http://www.chemcraftprog.com>.
- [31] Avci D (2011) Second and third-order nonlinear optical properties and molecular parameters of azo chromophores: semiempirical analysis. *Spectrochim. Acta A.* 82: 37-43. doi: 10.1016/j.saa.2011.06.037
- [32] Avci D, Başoğlu A, Atalay Y (2013) NLO and NBO Analysis of Sarcosine Maleic Acid by Using HF and B3LYP Calculations, Hindawi Publishing Corporation *J. Chem.* Article ID 712130: 1-16. doi: 10.1155/2013/712130
- [33] Tomasz S, Katarzyna S, Benoît C (2014): Ab initio Hartree-Fock calculations on linear and second-order nonlinear optical properties of ionic organic crystals, *J. Chem. Phys.* 141: 104109. doi: 10.1063/1.4894483
- [34] Jean-Luc Adam, (2002) Lanthanides in Non-Oxide Glasses. *Chem. Rev.* 102: 2461-2476. doi: 10.1021/cr010305b
- [35] Yanai T, Tew D, and Handy N, (2004) A new hybrid exchange-correlation functional using the Coulomb-attenuating method (CAM-B3LYP). *Chem. Phys. Lett.* 393: 51-57. doi: <https://doi.org/10.1016/j.cplett.2004.06.011>
- [36] Chocholoušová J, Špirko V, Hobza P, (2004) First local minimum of the formic acid dimer exhibits simultaneously red-shifted O-H...O and improper blue-shifted C-H...O hydrogen bonds. *Phys. Chem. Chem. Phys.* 6: 37-41. doi: 10.1039/B314148A
- [37] Szafran M., Komasa A., Bartoszak-Adamska E., (2007) Crystal and molecular structure of 4-carboxypiperidinium chloride (4-piperidinecarboxylic acid hydrochloride). *J. Mol. Struct.* 827:101-107. doi: 10.1016/j.molstruc.2006.05.012
- [38] Gamal A. El-Hiti, Keith Smith, Amany S. Hegazy, Ali M. Masmali and Benson M. Kariuki, (2014) Crystal structure of 2-tert-butyl-1,3-thiazolo[4,5-b]pyridine. *Acta Cryst.* E70: 932-937. doi:10.1107/S160053681401633X
- [39] Gamal A. El-Hiti, Keith Smith, Amany S. Hegazy, Saud A. Alanazi and Benson M. Kariuki, (2015) Crystal structure of 2-(2-methylphenyl)-1,3-thiazolo[4,5-b]pyridine. *Acta Cryst.* E71: 562-563. doi: 10.1107/S2056989015012797
- [40] Gamal A. El-Hiti, Keith Smith, Amany S. Hegazy, Mansour D. Ajarim, Benson M. Kariuki (2015) Crystal structure of 2-(3-nitrophenyl)-1,3-thiazolo[4,5-b]pyridine. *Acta Cryst.* E71: 0877-882. doi: 10.1107/S2056989015019118
- [41] Reddy C, Rao D, Yakub V, Nagaraj A (2010) Synthesis and in vitro Study of Some New Bis(thiadiazolyl-2H-pyrazolo[3,4-d][1,3]thiazole)-methanes as Potential Nematicides, *Acta Chim. Slov.* 57: 798-807. doi: [acta-arhiv.chem-soc.si/57/57-4-798.pdf](https://doi.org/10.2478/acta-arhiv.chem-soc.si/57/57-4-798.pdf)
- [42] Natorajan S, Shanmugam G, and MartinCryst SA, (2008) *Res. Technol.* 43: 561; Chemia D. S, Zysss J (1987) *Nonlinear Optical Properties of Organic Molecules and Crystals* Academic Press, Orlando, FL, Bradshaw D. S, Andrews D. L (2009) *J. Nonlinear Opt. Phys. Matter* 18: 285. Sures S (2013) The Growth and the Optical, Mechanical, Dielectric and Photoconductivity Properties of a New Nonlinear Optical Crystal—L-Phenylalanine-4-nitrophenol NLO Single Crystal Scientific-Research An Academic Publisher1, 3: 87-91 doi: 10.4236/jcpt.2013.33014
- [43] Cheng LT, Tam W, Stevenson SH, Meredith GR, Rikken G, Marder SR (1991) Electric field induced second harmonic generation with and without fringes, *J. Phys. Chem.* 95: 10631. doi: <https://doi.org/10.1021/jp00014a011>
- [44] Kaatz P, Donley EA, Shelton DP (1998) Analysis of nonlinear optical properties in donor-acceptor materials, *J. Chem. Phys.* 108: 849. doi: <https://doi.org/10.1063/1.475448>, Citation, CAS.
- [45] Gnanasambandan T, Gunasekaran S, Seshadri S (2014) Experimental and theoretical study of p-nitroacetanilide. *Spectrochimica. Acta Part A: Molecular and Biomolecular Spectroscopy* 117: 557-567. doi: <https://doi.org/10.1016/j.saa.2013.08.061>
- [46] Murray JS, Sen K (1996) *Molecular Electrostatic Potentials, Concepts and Applications*, Elsevier, Amsterdam 7 and Sicrocco E, Tomasi J, (1978) *Electronic Molecular Structure, Reactivity and Intermolecular Forces: An Euristic Interpretation by Means of Electrostatic Molecular Potentials*, *Adv. Quant. Chem.* 11: 115-193. doi: [https://doi.org/10.1016/S0065-3276\(08\)60236-1](https://doi.org/10.1016/S0065-3276(08)60236-1)
- [47] Politzer P, Murray JS (2002) The fundamental nature and role of the electrostatic potential in atoms and molecules. *Theor. Chem. Acc.* 108: 134-142. doi:10.1007/s00214-002-0363-9
- [48] Sajan D, Joseph L, Vijayan N, Karabacak M (2011) Natural bond orbital analysis, electronic structure, non-linear properties and vibrational spectral analysis of l-histidinium bromide monohydrate: A density functional theory *Spectrochim. Acta A.* 81: 85-98. doi: 10.1016/j.saa.2011.05.052